Cell Reports

p53 Suppresses Metabolic Stress-Induced Ferroptosis in Cancer Cells

Graphical Abstract

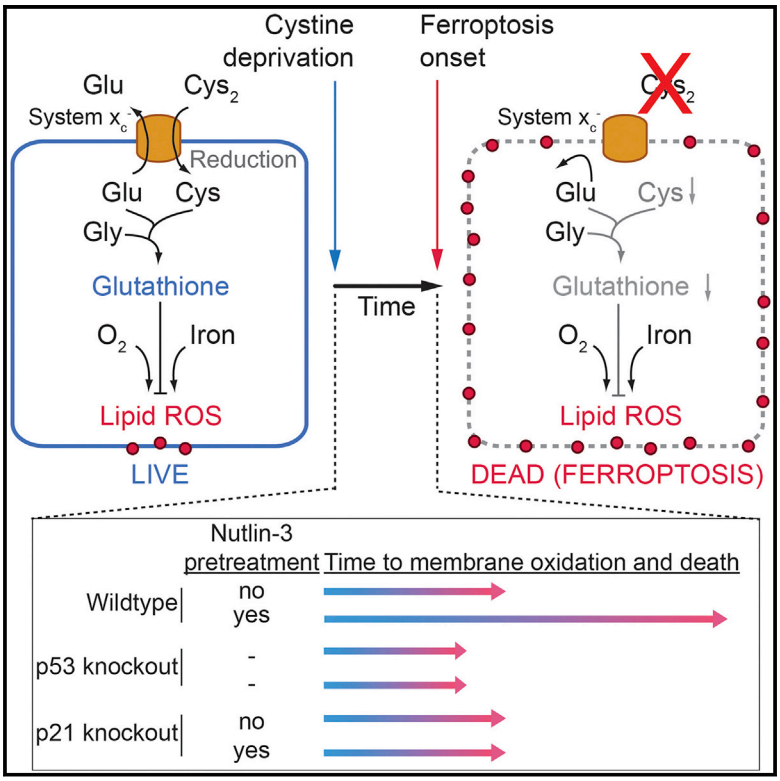

Highlights

- p53 stabilization can delay the induction of ferroptosis in cancer cells
- This effect requires the p53 transcriptional target gene *CDKN1A* (p21)
- Cell-cycle arrest per se may not be sufficient to inhibit ferroptosis
- Inhibition of ferroptosis correlates with conservation of glutathione

Authors

Amy Tarangelo, Leslie Magtanong, Kathryn T. Bieging-Rolett, Yang Li, Jiangbin Ye, Laura D. Attardi, Scott J. Dixon

Correspondence

sjdixon@stanford.edu

In Brief

Tarangelo et al. show that stabilization of wild-type p53, leading to expression of the downstream target *CDKN1A* (encoding $p21^{CIP1/WAF1}$), delays the onset of ferroptosis in response to subsequent cystine deprivation in human and in mouse cancer cells.

Tarangelo et al., 2018, Cell Reports *22*, 569–575
January 16, 2018
https://doi.org/10.1016/j.celrep.2017.12.077

CellPress

Cell Reports
Report

p53 Suppresses Metabolic Stress-Induced Ferroptosis in Cancer Cells

Amy Tarangelo,[1] Leslie Magtanong,[4] Kathryn T. Bieging-Rolett,[2] Yang Li,[1,2] Jiangbin Ye,[1,2] Laura D. Attardi,[1,2,3] and Scott J. Dixon[1,4,5,*]
[1]Program in Cancer Biology
[2]Department of Radiation Oncology
[3]Department of Genetics
Stanford University School of Medicine, 291 Campus Drive, Stanford, CA 94305, USA
[4]Department of Biology, Stanford University, 337 Campus Drive, Stanford, CA 94305, USA
[5]Lead Contact
*Correspondence: sjdixon@stanford.edu
https://doi.org/10.1016/j.celrep.2017.12.077

SUMMARY

How cancer cells respond to nutrient deprivation remains poorly understood. In certain cancer cells, deprivation of cystine induces a non-apoptotic, iron-dependent form of cell death termed ferroptosis. Recent evidence suggests that ferroptosis sensitivity may be modulated by the stress-responsive transcription factor and canonical tumor suppressor protein p53. Using CRISPR/Cas9 genome editing, small-molecule probes, and high-resolution, time-lapse imaging, we find that stabilization of wild-type p53 delays the onset of ferroptosis in response to cystine deprivation. This delay requires the p53 transcriptional target *CDKN1A* (encoding p21) and is associated with both slower depletion of intracellular glutathione and a reduced accumulation of toxic lipid-reactive oxygen species (ROS). Thus, the p53-p21 axis may help cancer cells cope with metabolic stress induced by cystine deprivation by delaying the onset of non-apoptotic cell death.

INTRODUCTION

The p53 tumor suppressor is mutated or functionally inactivated in many tumors (Bieging et al., 2014; Pfister and Prives, 2017). How wild-type p53 suppresses tumor formation remains unclear despite decades of study. Recently, acetylation-defective p53 mutants were shown to promote ferroptosis, an iron-dependent, oxidative and non-apoptotic form of cell death (Jiang et al., 2015; Wang et al., 2016). These p53 mutants are unable to induce apoptosis, cell-cycle arrest, or senescence, yet retain the ability to prevent tumor formation in mice (Li et al., 2012), suggesting that p53-induced ferroptosis could be responsible for tumor suppression. However, other results suggest that p53 expression may inhibit ferroptosis in certain cells, either through a post-translational mechanism (Xie et al., 2017) or via effects on the transcription of metabolic genes (Jennis et al., 2016). Thus, the impact of p53 expression on ferroptosis sensitivity is poorly understood.

System x_c^- is a cystine/glutamate antiporter whose constitutive activity suppresses ferroptosis in many cell types (Dixon et al., 2012; Stockwell et al., 2017). System x_c^--mediated cystine import is necessary for the synthesis of the antioxidant tripeptide (reduced) glutathione (GSH). Depletion of cystine and/or GSH results in the iron-dependent accumulation of lethal lipid-reactive oxygen species (ROS), a process that is suppressed by lipophilic antioxidants such as ferrostatin-1 (Dixon et al., 2012; Stockwell et al., 2017). Here, we examined the relationship between wild-type p53 expression and ferroptosis sensitivity in response to system x_c^- inhibition. We find that wild-type p53 stabilization can decrease system x_c^- activity yet simultaneously reduce ferroptosis sensitivity in a broad range of cell types. This protective effect requires expression of the p53 transcriptional target *CDKN1A* (encoding p21) and conservation of intracellular GSH. These results indicate that the p53-p21 transcriptional axis negatively regulates ferroptosis in cancer cells.

RESULTS

p53 Stabilization Suppresses Ferroptosis in Response to System x_c^- Inhibition

Human HT-1080 fibrosarcoma cells are a classic ferroptosis model that express wild-type p53 (Dixon et al., 2012; Stockwell et al., 2017; Tarunina and Jenkins, 1993). To characterize the effects of p53 expression on ferroptosis in these cells, we used CRISPR/Cas9 technology to isolate a clonal *TP53* knockout ($TP53^{KO}$) cell line. The small-molecule MDM2 inhibitor nutlin-3 (10 μM, 48 hr) increased p53 levels, upregulated the canonical p53 target genes *CDKN1A* and *MDM2*, and induced G1 cell-cycle arrest in parental (control) cells, but not in $TP53^{KO}$ cells, suggesting that $TP53^{KO}$ cells lacked p53 function (Figures 1A–1C). To determine how p53 expression affected ferroptosis sensitivity, we examined control and $TP53^{KO}$ cells pretreated for 48 hr with or without nutlin-3, then treated for a further 48 hr with or without the potent and specific system x_c^- inhibitor erastin2 (Dixon et al., 2014) (Figure 1D). Cell death was quantified during this second phase using scalable time-lapse analysis of cell death kinetics (STACK), an imaging-based method that measures cell death within a population over time (Forcina et al., 2017). We observed that control cells pretreated with nutlin-3

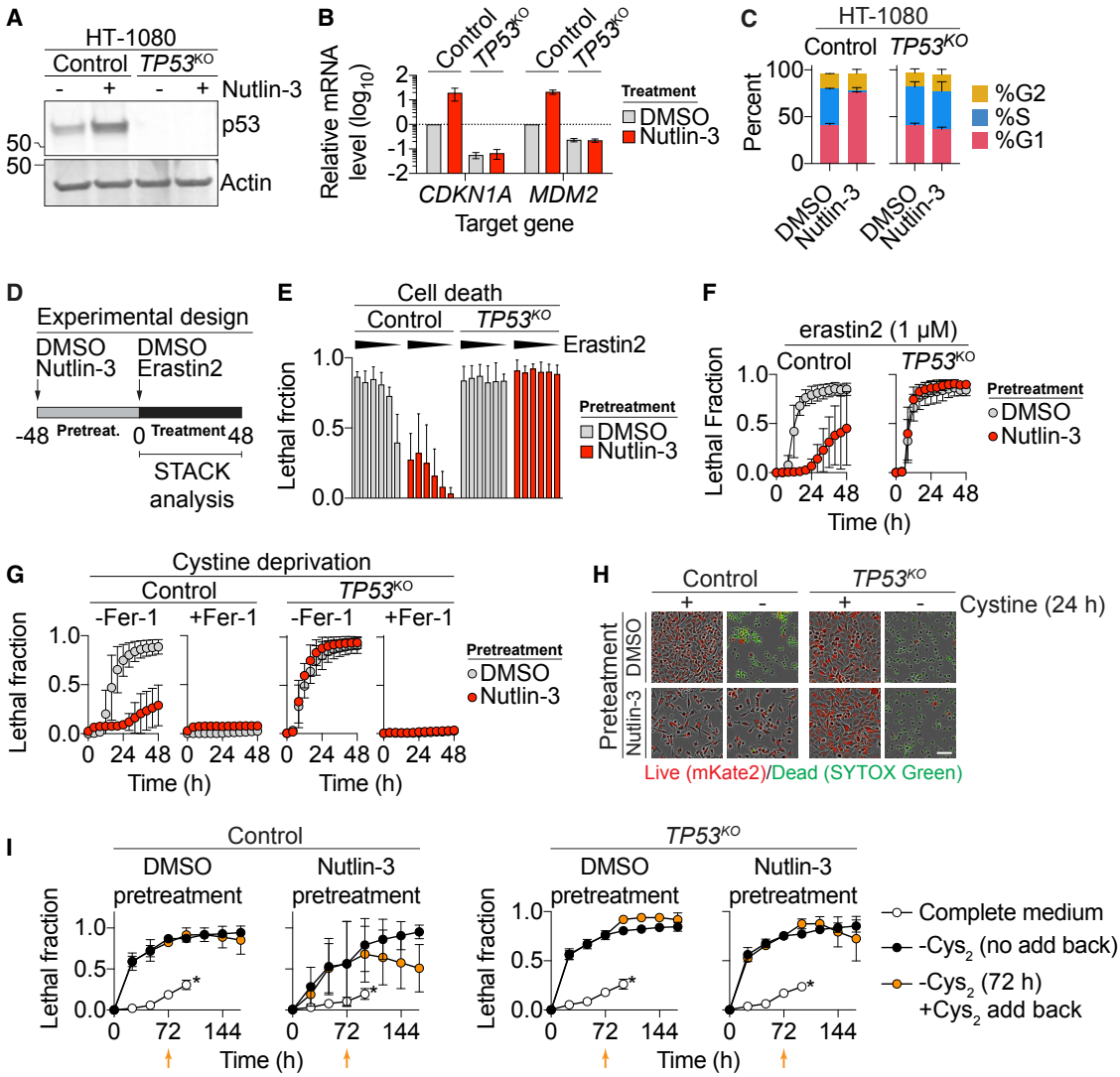

Figure 1. p53 Suppresses Ferroptosis

(A) p53 levels determined by immunoblotting.

(B) Expression of p53 target genes ± nutlin-3 (10 μM, 48 hr).

(C) Cell-cycle profiles ± nutlin-3 (10 μM, 48 hr).

(D) Standard cell death experimental design, involving an unobserved 48-hr pretreatment phase and a 48-hr compound treatment phase, where cell death was measured using scalable time-lapse analysis of cell death kinetics (STACK).

(E) Cell death (lethal fraction) at 36 hr of erastin2 treatment. Erastin2 was tested in a 6-point, 2-fold dose-response series (indicated by black triangle), with a high concentration of 2 μM. On the y axis, 0 = all cells alive and 1 = all cells dead.

(F and G) Cell death over time in response to erastin2 (F) and cystine deprivation (G) following pretreatment with or without (10 μM, 48 hr) .

(H) Representative images from (G). Scale bar, 25 μm.

(I) Cell death over time. Orange data points represent cells transiently (72 hr) deprived of cystine (Cys_2) followed by Cys_2 restoration. Orange arrows indicate the time point of Cys_2 add back. An asterisk indicates cells maintained in cystine-containing medium; time courses were terminated at 96 hr due to high-population confluence.

Data represent mean ± SD from at least three independent biological replicates (B, C, E–G, and I).

were less sensitive to erastin2-induced cell death, both across erastin2 concentrations and over time (Figures 1E and 1F). By contrast, *TP53*^{KO} cells were equally sensitive to erastin2 regardless of nutlin-3 pretreatment (Figures 1E and 1F). The protective effect of nutlin-3 pretreatment on subsequent erastin2-induced cell death could also be detected in HT-1080 cells using an alternative measure of cell viability, the metabolic indicator PrestoBlue (Figure S1A).

We next tested the generalizability of the findings obtained in HT-1080 cells to other cell types. Similar to HT-1080 cells, nutlin-3 pretreatment increased the expression of canonical p53 target genes and transiently suppressed erastin2-induced

ferroptosis in *Trp53*$^{+/+}$, but not in *Trp53*$^{-/-}$, primary mouse embryonic fibroblasts (Figures S1B and S1C). Nutlin-3 pretreatment also increased p53 protein levels in p53 wild-type U-2 OS, ACHN, Caki-1, and A549 cells without causing substantial cell death alone, and delayed the onset of erastin2-induced ferroptosis (Figures S1D–S1F). SJSA-1 cells express wild-type p53 and are susceptible to nutlin-3-induced apoptosis (Vassilev et al., 2004). In these cells, a 24 hr nutlin-3 pretreatment elevated p53 levels and suppressed erastin2-induced cell death to the level of cell death observed with nutlin-3 alone, indicating that p53 stabilization may be capable of inducing apoptosis and suppressing ferroptosis simultaneously (Figures S2A–S2C). Nutlin-3 pretreatment had weaker effects on erastin2-induced ferroptosis in p53 null H1299 cells and p53 mutant T98G cells, consistent with a requirement for wild-type p53 expression and stabilization for suppression of erastin2-induced ferroptosis in cancer cells (Figures S1D–S1F). However, in non-cancerous IMR-90 human fetal lung fibroblasts that express wild-type p53, nutlin-3 pretreatment elevated p53 levels without altering the onset of erastin2-induced ferroptosis, indicating that the association of p53 stabilization with protection against ferroptosis is not universal (Figures S2D and S2E).

While erastin2 inhibits system x_c^- function (Dixon et al., 2014), it could potentially have other effects on the cell. To address this point, HT-1080 control and *TP53*^{KO} cells were pretreated with nutlin-3 or DMSO then directly cultured in medium lacking cystine. Under these conditions, nutlin-3 pretreatment suppressed the death of control cells, but not *TP53*^{KO} cells (Figures 1G and 1H; note that nutlin-3 treatment alone was not lethal to either cell line). Cell death in response to cystine deprivation was completely blocked by a potent and specific antioxidant inhibitor of ferroptosis, ferrostatin-1 (Fer-1, 2 μM) (Dixon et al., 2012) (Figure 1G). Erastin2-induced death was likewise completely suppressed by co-treatment with a structurally distinct nitroxide-based free radical scavenger (Figure S2F), indicating that nutlin-3 pretreatment does not alter the mode of cell death caused by cystine deprivation or erastin2 treatment.

Using the cystine deprivation paradigm, we examined the ability of p53 stabilization to promote long-term cell survival. We pretreated HT-1080 control and *TP53*^{KO} cells with DMSO or nutlin-3, then deprived cells of cystine for 72 hr in the continued presence of DMSO or nutlin-3, at which point cystine was restored (without DMSO or nutlin-3) and cell viability examined over the following 96 hr. Nutlin-3 pretreatment delayed the onset of cell death over the 72-hr cystine deprivation period in control versus *TP53*^{KO} cells, as expected (Figure 1I). Moreover, upon cystine restoration, only nutlin-3-pretreated control cells exhibited a steady decrease in the lethal fraction over time, which is best explained by an increase in the number of live cells within the population (Forcina et al., 2017) (Figure 1I, orange datapoints). Collectively, these results suggest that p53 stabilization promotes cell survival in response to cystine deprivation by blocking ferroptosis.

Delayed Ferroptosis Onset Requires p21

p53 may impact ferroptosis via transcriptional or posttranslational mechanisms (Jennis et al., 2016; Jiang et al., 2015; Xie et al., 2017). In HT-1080 cells, more than 12 hr of nutlin-3 pretreatment were required to delay the onset of erastin2-induced ferroptosis, which suggested a p53-dependent transcriptional effect (Figure S3A). To investigate this further, we isolated lung adenocarcinoma cell lines derived from *Kras*$^{LA2/+}$; *Trp53*$^{LSL\text{-}wt/LSL\text{-}wt}$ (KP^{WT}) and *Kras*$^{LA2/+}$; *Trp53*$^{LSL\text{-}25,26/LSL\text{-}25,26}$ (KP^{25,26}) mice (Johnson et al., 2001, 2005). KP^{WT} and KP^{25,26} cells express oncogenic Kras^{G12D}. When infected with a virus directing the expression of Cre recombinase (Ad-Cre), but not a control adenovirus (Ad-empty), these cells re-expressed wild-type p53, upregulated the p53 target genes *Mdm2* and *Cdkn1a*, and exhibited reduced sensitivity to erastin2-induced, Fer-1-sensitive cell death (Figures 2A, 2B, S3B, and S3C). Ad-Cre infected KP^{25,26} cells re-express a mutant p53 protein (i.e., p53^{25,26}) that cannot robustly transactivate most canonical p53 target genes including *Cdkn1a* (Brady et al., 2011) (Figures S3D and S3E). In Ad-Cre-infected KP^{25,26} cells, erastin2-induced ferroptosis was not suppressed (Figures 2C). Thus, transcriptional upregulation of one or more p53 target genes appeared essential to suppress ferroptosis.

CDKN1A (encoding p21) is a key transcriptional target of p53 that can inhibit cell-cycle progression and impact glutathione metabolism, making it a logical candidate to examine in the context of ferroptosis (Abbas and Dutta, 2009; Maddocks et al., 2013). Nutlin-3 treatment resulted in upregulation of *CDKN1A* mRNA and p21 protein in control but not *TP53*^{KO} HT-1080 cells, consistent with a possible role in ferroptosis regulation (Figures 1B and 2D). We therefore used CRISPR to generate two independent clonal HT-1080 *CDKN1A*^{KO} cell lines that lacked p21 expression and failed to undergo nutlin-3-induced cell-cycle arrest despite normal stabilization of p53 and upregulation of the p53 target gene *MDM2* (Figures 2D–2F). Strikingly, and in contrast to control cells, nutlin-3 pretreatment conferred essentially no protection against erastin2-induced cell death in *CDKN1A*$^{KO1/2}$ cells, either across compound doses or over time (Figures 2G and 2H). Short hairpin RNA (shRNA)-mediated silencing of *CDKN1A* in Caki-1 cells likewise abrogated the ability of nutlin-3 pretreatment to delay subsequent erastin2-induced cell death (Figures S3F and S3G). These results suggest a requirement for p21, downstream of p53, to suppress ferroptosis in response to system x_c^- inhibition.

p21 causes cell-cycle arrest by inhibiting the activity of cyclin-dependent kinase (CDK) complexes that contain the G_1/S kinases CDK2, CDK4 and CDK6 (Abbas and Dutta, 2009). We investigated whether cell-cycle arrest was sufficient to protect against ferroptosis. Lentiviral overexpression of *CDKN1A* in HT-1080 cells delayed the onset of erastin2-induced ferroptosis relative to cells transduced with an empty control virus (Figures S3H and S3I). To test whether cell-cycle arrest per se was sufficient to suppress ferroptosis, we inhibited cell-cycle progression downstream of p21 at the level of CDK4/6. Inhibition of CDK4/6 function using the specific inhibitor palbociclib (2 μM, 48 hr) arrested the proliferation of both control and *TP53*^{KO} HT-1080 cells, predominantly in G1 (Figures 2I and 2J). However, pretreatment with palbociclib did not alter the sensitivity of either control or *TP53*^{KO} cells to erastin2-induced ferroptosis (Figure 2J). Thus, cell-cycle arrest caused by CDK4/6 inhibition does not appear to be sufficient to inhibit ferroptosis.

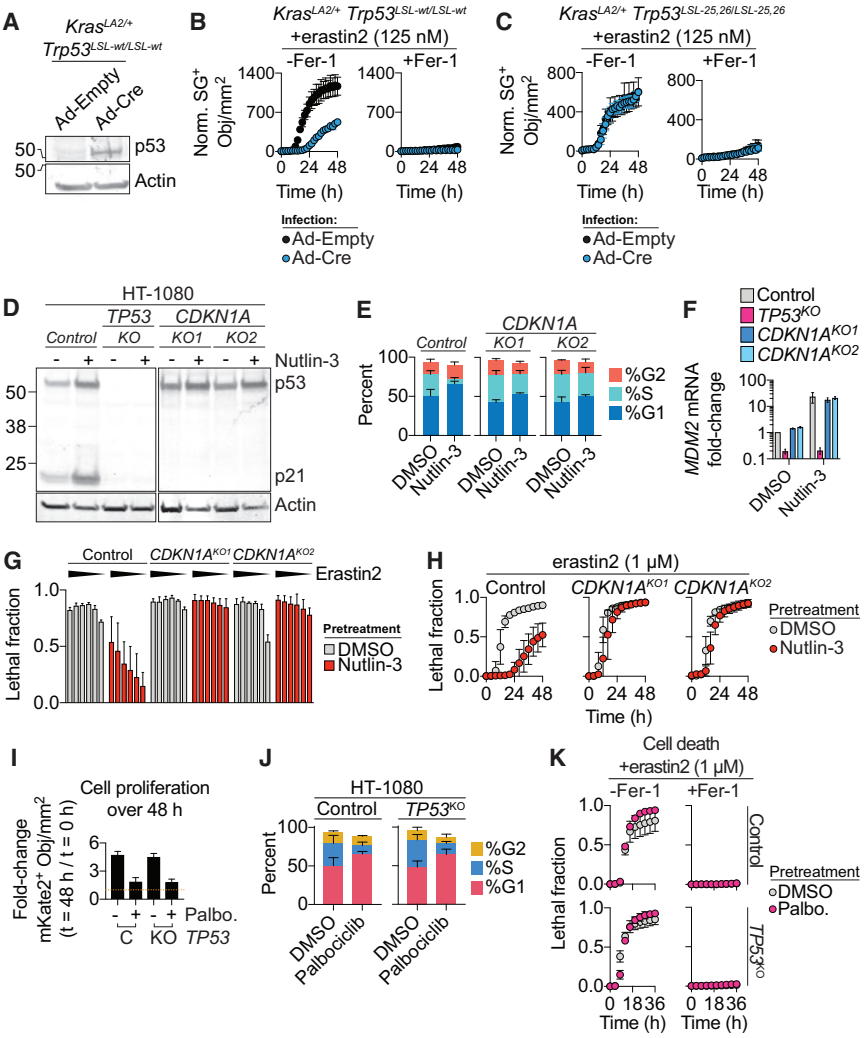

Figure 2. Effect of Genetic Manipulation of p53 Levels on Ferroptosis

(A) p53 expression in $Kras^{LA2/+};Trp53^{LSL\text{-}wt/LSL\text{-}wt}$ mouse lung adenocarcinoma cells following infection with empty adenovirus (Ad-empty) or adenovirus directing the expression of Cre recombinase (Ad-Cre).

(B and C) Normalized SYTOX Green (norm. SG^+) dead cell counts over time in KP^{WT} (B) and $KP^{25,26}$ (C) cells infected with Ad-empty or Ad-Cre cells prior to treatment with erastin2 ± ferrostatin-1 (Fer-1, 2 μM).

(D) p53 and p21 levels determined by immunoblotting.

(E and F) Cell-cycle profile (E) and *MDM2* expression (F) in control and $CDKN1A^{KO1/2}$ cell lines ± nutlin-3.

(G) Cell death following erastin2 treatment (36 hr). Erastin2 was tested in a 6-point, 2-fold dose-response series (black traingles) starting at 4 μM.

(H) Cell death over time in response to erastin2.

(I) Cell proliferation expressed as the fold change in live cell ($mKate2^+$) counts over 48 hr in HT-1080 control (C) and $TP53^{KO}$ (KO) cells ± palbociclib (Palbo., 2 μM). The yellow dotted line indicates a ratio of 1 (e.g., no change).

(J) Cell-cycle profiles ± palbociclib (2 μM, 48 hr).

(K) Cell death over time in cells pretreated ± palbociclib and then treated with erastin2 ± ferrostatin-1 (Fer-1, 2 μM).

Data represent mean ± SD from at least three independent biological replicates (B, C, and E–K).

inducer of xCT expression, *tert*-butylhydroquinone (tBHQ, 100 μM, 48 hr [Lewerenz et al., 2012]) increased xCT/*SLC7A11* levels, validating our reagents (Figures 3D and 3E).

We reasoned that the inhibitory effect of p53 stabilization on system x_c^- function must be counterbalanced by other alterations that ultimately reduce cellular ferroptosis sensitivity. The antioxidant master regulator transcription factor NFE 2-like 2 (NRF2) can be activated by p21 (Chen et al., 2009), and we wondered whether p21-stimulated NRF2 activity and antioxidant gene expression could be compromised by disruption of the p53-p21 axis. However, tBHQ, a bona fide inducer of NRF2 activity (Lewerenz et al., 2012), stimulated the expression of two canonical NRF2 target genes, *HMOX1* and *GCLM*, equally in control, $TP53^{KO}$ and $CDKN1A^{KO1/2}$ cells (Figure 3F). Conversely, nutlin-3 treatment did not consistently enhance *HMOX1* and *GCLM* expression in these cells (Figure 3F). Thus, it appeared unlikely that the p53-p21 axis suppressed ferroptosis by enhancing NRF2 activity.

p53 Stabilization Can Decrease System x_c^- Activity

Ferroptosis is inhibited by system x_c^- activity (Stockwell et al., 2017), and acetylation-defective p53 mutants sensitize to ferroptosis by repressing *SLC7A11*/xCT expression and system x_c^- function (Jiang et al., 2015). Indeed, direct small interfering RNA (siRNA)-mediated silencing of *SLC7A11* expression sensitized HT-1080 cells to erastin2-induced cell death (Figures 3A and 3B). We therefore examined how stabilization of wild-type p53, which protects from cell death (e.g., Figures 1 and 2), altered xCT/*SLC7A11* expression and system x_c^- function. In HT-1080 control cells basal system x_c^- activity (i.e., Na^+-independent glutamate release [Dixon et al., 2014]), xCT protein levels and *SLC7A11* mRNA expression were all reduced by nutlin-3 treatment (Figures 3C–3E). System x_c^- activity and *SLC7A11*/xCT expression were lower in $TP53^{KO}$ cells and insensitive to nutlin-3 (Figures 3C–3E). These effects may be due to reorganization of metabolic networks in mutant cells to compensate for the loss of p53. In both cell lines, system x_c^- activity was fully inhibited by treatment with erastin2 (1 μM, 2 hr), confirming the specificity of this assay (Figure 3C). A known

p53 Stabilization Leads to Conservation of Intracellular Glutathione

The toxic lipid ROS accumulation occurring during ferroptosis can be monitored using the lipid ROS probe C11 BODIPY 581/591 (Dixon et al., 2012). HT-1080 cells pretreated with DMSO and then treated with erastin2 (1 μM, 10 hr) exhibited robust

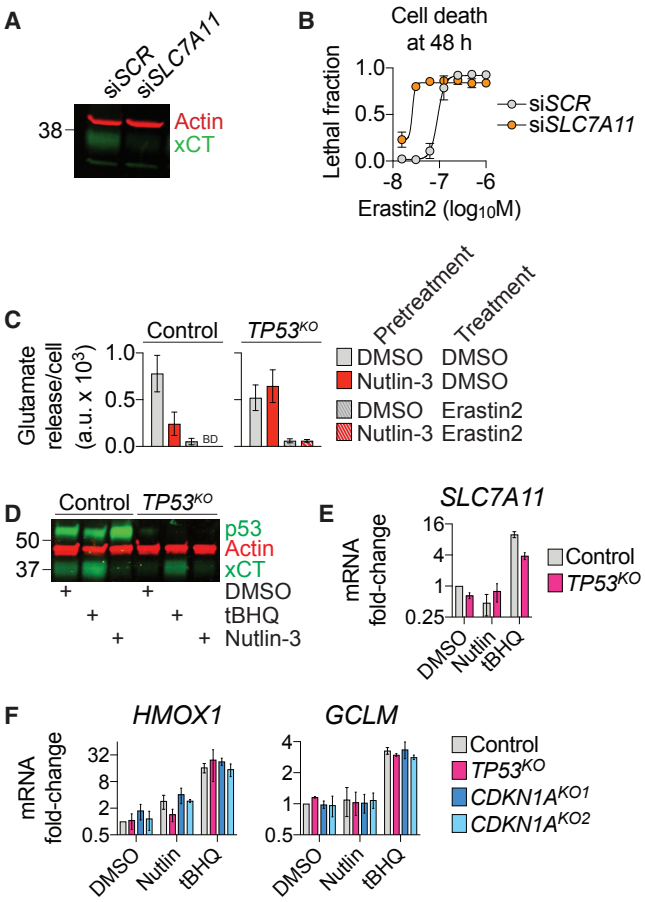

Figure 3. p53 Stabilization affects System x_c^-

(A) xCT levels following transfection (48 hr) with scrambled (SCR) siRNA or siRNA-targeting *SLC7A11*.

(B) Erastin2 dose-response at 48 hr, following 48 hr after transfection with siRNAs like in (A).

(C) Glutamate release, a measure of system x_c^- activity ± erastin2 (1 μM) following pretreatment ± nutlin-3. BD: below limit of detection.

(D) p53 and xCT protein levels following DMSO, *tert*-butylhydroquinone (tBHQ, 100 μM), or nutlin-3 (10 μM) treatment for 48 hr.

(E and F) *SLC7A11* (E) and *HMOX* and *GCLM* (F) mRNA expression following DMSO (vehicle), nutlin-3 (10 μM), or tBHQ (100 μM) treatment for 48 hr.

Data represent mean ± SD from at least three independent biological replicates (B, C, E, and F).

probe oxidation, both on internal membranes and in a distinct ring around the periphery of the cell (Figure 4A). Pretreatment with nutlin-3 reduced probe oxidation upon subsequent erastin2 treatment in both locations (Figure 4A). Lipid ROS accumulation is opposed by GPX4, a (reduced) glutathione (GSH)-dependent lipid hydroperoxidase (Stockwell et al., 2017). In control HT-1080 cells, total glutathione levels (as determined using Ellman's reagent) were not elevated by nutlin-3 pretreatment (Figure 4B). Notably, however, nutlin-3-pretreated control cells exhibited higher glutathione levels than control cells pretreated with DMSO, or *TP53*^{KO} or *CDKN1A*$^{KO1/2}$ cells pretreated with DMSO or nutlin-3, following erastin2 treatment (1 μM, 8 hr) (Figures 4B and S4A).

Based on these results, we investigated whether p53 stabilization delayed ferroptosis by limiting GSH depletion or enhancing GSH synthesis using mass spectrometry and carbon-13 labeling. HT-1080 control and *TP53*^{KO} cells were pretreated with either DMSO or nutlin-3 for 48 hr and then incubated in the presence or absence of erastin2 (1 μM) for 8 hr in medium containing uniformly (U) labeled-^{13}C-serine. Within the cell, serine can be converted into glycine, which is then directly incorporated into GSH via *de novo* synthesis, yielding GSH M+2 (Figure 4C). Serine also can be utilized in the synthesis of cysteine via the transsulfuration pathway, ultimately resulting in GSH M+5 (via glycine and transsulfuration; Figure 4C). In control and *TP53*^{KO} cells, most intracellular serine was labeled (M+3) at 8 hr, and this labeling was not grossly affected by nutlin-3 or erastin2, indicating that these treatments did not affect the uptake of the tracer (Figure S4B). In control cells, nutlin-3 pretreatment resulted in higher levels of total GSH (all isotopologues) following erastin2 treatment compared to cells pretreated with DMSO, or compared to *TP53*^{KO} cells pretreated with DMSO or nutlin-3 (Figure 4D). GSSG represented a minor fraction of the total glutathione in control (< 10%) and *TP53*^{KO} (< 20%) cells and was unaffected by nutlin-3 pretreatment, indicating that higher levels of GSH likely account for the increase in total glutathione.

Examining the distribution of GSH isotopologues, we observed that *de novo* GSH synthesis was inhibited in control cells pretreated with nutlin-3, as indicated by a reduction in GSH M+2 relative to control cells pretreated with DMSO (Figure 4E). This effect was not observed in *TP53*^{KO} cells pretreated with either nutlin-3 or DMSO (Figure 4E). In control cells pretreated with nutlin-3, most of the GSH retained upon erastin2 treatment was the unlabeled M+0 species, suggesting that it was derived from preexisting pools rather than *de novo* (i.e., stress-induced) synthesis. Under no conditions did we observe accumulation of GSH M+5, indicating that the transsulfuration pathway was not active in these cells (Figure 4E). Based on these results, we predicted that GSH synthesized during the pretreatment phase (i.e., detected as GSH M+0 in our experiments) was important for the protective effect of p53 stabilization in response to system x_c^- inhibition. Consistent with this prediction, addition of the GSH biosynthesis inhibitor buthionine sulfoximine (BSO, 100 μM, 24 hr) during the nutlin-3 pretreatment phase, but not the erastin2 treatment phase, sensitized control HT-1080 cells to ferroptosis, regardless of nutlin-3 pretreatment (Figure 4F).

DISCUSSION

Depending on the context, p53 can either promote or prevent cell death (Kruiswijk et al., 2015; Paek et al., 2016). We find that prolonged (>24 hr) stabilization of wild-type p53 renders many cancer cells less sensitive to ferroptosis induced by system x_c^- inhibition or direct cystine deprivation. This reduced sensitivity to ferroptosis requires p21 and the conservation of intracellular GSH (Figure S4C). How activation of the p53-p21 axis reduces cellular reliance on system x_c^--mediated cystine import and ongoing *de novo* GSH synthesis is unclear. p21 inhibits cell-cycle progression (Abbas and Dutta, 2009), but experiments using the CDK4/6 inhibitor palbociclib tentatively suggest

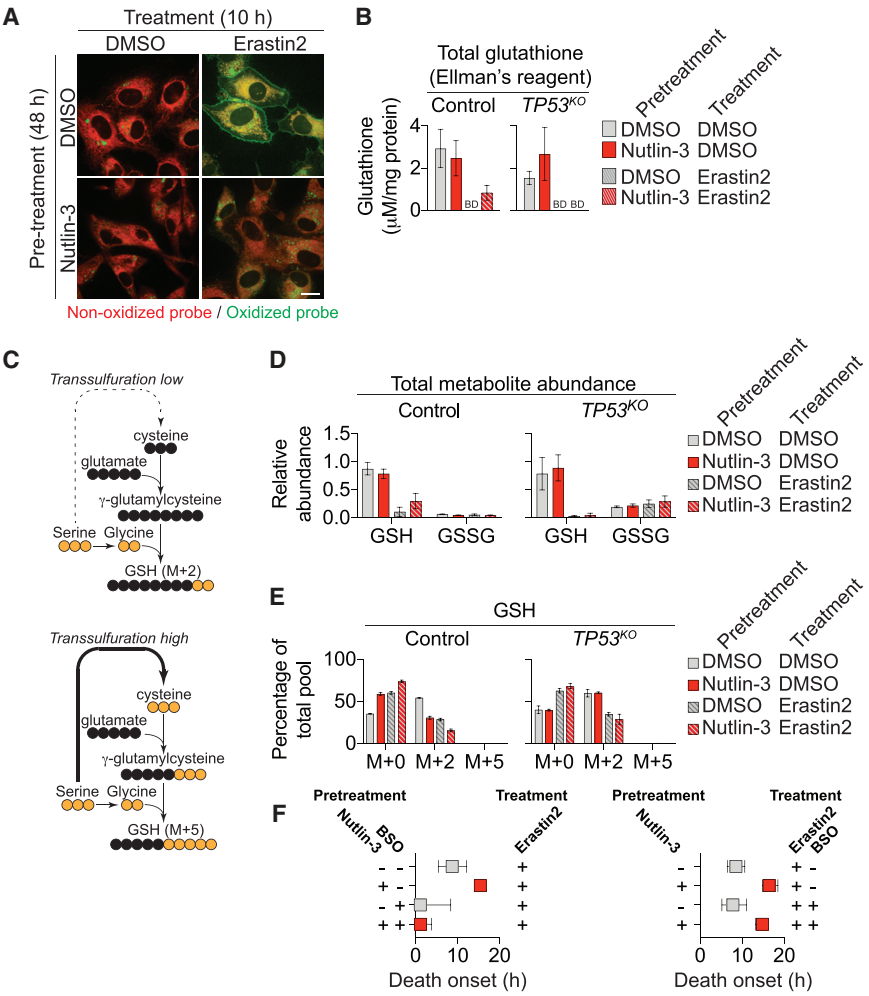

Figure 4. p53 Expression Alters GSH Metabolism

(A) C11 BODIPY 581/591 labeling in HT-1080 cells. Scale bar, 15 μm.

(B) Total glutathione levels ± nutlin-3 pretreatment ± erastin2 (1 μM, 8 hr). BD, below the limit of detection.

(C) Outline of carbon flux in metabolic pathways leading from uniformly (U) labeled ^{13}C-serine (yellow) to GSH. The dotted line indicates multiple steps (data not shown) in the pathway from serine to cystine via transsulfuration. Also not shown is the flux of (unlabeled) cysteine from system x_c^--dependent cystine uptake.

(D) Relative metabolite abundance (all isotopologues) determined by mass spectrometry ± nutlin-3 pretreatment ± erastin2 (1 μM, 8 hr). U-^{13}C-serine was added only during the 8-hr treatment phase.

(E) Isotopologues of GSH detected in the experiment outlined in (D).

(F) Effects of buthionine sulfoximine (BSO, 100 μM) inclusion during the pretreatment (left) or treatment (right) phases on erastin2-induced cell death. The timing of initial population cell death onset is extracted from curves of cell death over time for each condition (see the Supplemental Experimental Procedures).

that inhibition of proliferation and cell-cycle arrest per se are insufficient to inhibit ferroptosis. It is possible that p21-dependent inhibition of additional or alternative CDKs (e.g., CDK1/2) is required to conserve GSH and inhibits ferroptosis through induction of a more complete cell-cycle arrest. Alternatively, p21 could potentially enhance GSH retention through effects on CDK-regulated metabolic enzymes (Ewald et al., 2016).

Our results are broadly consistent with the recent findings that ferroptosis is inhibited by basal p53 expression in colorectal cancer cells (Xie et al., 2017), but suggest a specific role for p53-mediated transcription and upregulation of p21 in the protective response conferred by p53 stabilization. Our results appear to contradict the findings that expression of acetylation-defective p53 mutants (i.e., 3KR) reduce system x_c^- function and sensitize cancer cells to ferroptosis (Jiang et al., 2015; Wang et al., 2016). However, acetylation-defective p53 mutants are unable to induce p21 (Jiang et al., 2015). We speculate that system x_c^- downregulation and p21 upregulation could be two branches of a coordinated p53-mediated response that normally decreases cystine import to match the lower metabolic demands of growth-arrested cells. One possibility is that such a coordinated response is modulated by acetylation and other p53 post-translational modifications (e.g., phosphorylation) (Jennis et al., 2016) to fine-tune ferroptosis sensitivity in specific contexts. Delaying the onset of ferroptosis by even a few hours could help a cancer cell survive transient exposure to harsh environmental conditions *in vivo*, such as the oxidizing conditions encountered in the bloodstream during metastasis (Piskounova et al., 2015). This could help explain why some cancers retain the ability to express wild-type p53 and p21.

Experimental Procedures

Further details and an outline of the resources used in this work can be found in the Supplemental Experimental Procedures.

Cell Lines

For cell viability studies, polyclonal Nuc::mKate2-expressing HT-1080 parental, *TP53*^{KO}, *CDKN1A*$^{KO1/2}$, U-2 OS, A549, T98G, H1299, ACHN, and CAKI-1 cell lines were generated by transducing parental cell lines with NucLight Red Lentivirus (Essen Bioscience) followed by selection with puromycin (1–2 μg/mL) for 4 days (Forcina et al., 2017). Murine lung tumor cell lines were generated by dissection of lung tumors from 11-week-old *Kras*$^{LA2/+}$;*Trp53*$^{LSL\text{-}wt/LSL\text{-}wt}$ and *Kras*$^{LA2/+}$;*Trp53*$^{LSL\text{-}25,26/LSL\text{-}25,26}$ male mice. Cultures were established in N5 medium supplemented with epidermal growth factor (EGF) (20 ng/mL) and fibroblast growth factor (FGF) (20 ng/mL), sorted by fluorescence-activated cell sorting (FACS) (Stanford Shared FACS facility) for EpCam positivity (BioLegend) and then switched to DMEM Hi-glucose media.

p53$^{+/+}$ and *p53*$^{-/-}$ mouse embryonic fibroblasts (MEFs) were isolated from E13.5 embryos as previously described (Johnson et al., 2005) and cultured in DMEM Hi-glucose media. All media were supplemented with 10% fetal bovine serum and 1× Pen/Strep (Life Technologies). All cell lines were grown at 37°C with 5% CO_2 in humidified tissue culture incubators (Thermo Scientific). All experiments involving cell isolation from tissues or embryos were performed in accordance with the Stanford APLAC #10382.

Data Analysis

Data were analyzed using Microsoft Excel and GraphPad Prism (v.6.0h) and are represented as mean ± SD or ± 95% confidence interval. Lethal fraction scoring was performed as using Microsoft Excel and GraphPad Prism, as previously described (Forcina et al., 2017).

SUPPLEMENTAL INFORMATION

Supplemental Information includes Supplemental Experimental Procedures and four figures and can be found with this article online at https://doi.org/10.1016/j.celrep.2017.12.077.

ACKNOWLEDGMENTS

We thank P.-J. Ko and T. Stearns for help with confocal imaging; J.-Y. Cao, C. Poltorack, and M. Morris for help with experiments; and J. Sage, J. Carette, and A. Gitler for providing reagents. This work was supported by an NSF GRFP fellowship (to A.T.), awards from the NIH (R35 CA197591 to L.D.A.; 4R00CA166517 and 1R01GM122923 to S.J.D.), and a Damon Runyon-Rachleff innovation award (to S.J.D.).

AUTHOR CONTRIBUTIONS

Conceptualization, A.T., L.D.A., and S.J.D.; Methodology, A.T., L.M., K.T.B.-R., and Y.L.; Investigation, A.T., L.M., and Y.L.; Writing - Original Draft, A.T. and S.J.D. Writing - Review & Editing, L.M., K.T.B.-R. and L.D.A. Funding Acquisition and Supervision, J.Y., L.D.A. and S.J.D.

DECLARATION OF INTERESTS

All authors declare no competing interests.

Received: June 26, 2017
Revised: November 15, 2017
Accepted: December 21, 2017
Published: January 16, 2018

REFERENCES

Abbas, T., and Dutta, A. (2009). p21 in cancer: intricate networks and multiple activities. Nat. Rev. Cancer *9*, 400–414.

Bieging, K.T., Mello, S.S., and Attardi, L.D. (2014). Unravelling mechanisms of p53-mediated tumour suppression. Nat. Rev. Cancer *14*, 359–370.

Brady, C.A., Jiang, D., Mello, S.S., Johnson, T.M., Jarvis, L.A., Kozak, M.M., Kenzelmann Broz, D., Basak, S., Park, E.J., McLaughlin, M.E., et al. (2011). Distinct p53 transcriptional programs dictate acute DNA-damage responses and tumor suppression. Cell *145*, 571–583.

Chen, W., Sun, Z., Wang, X.-J., Jiang, T., Huang, Z., Fang, D., and Zhang, D.D. (2009). Direct interaction between Nrf2 and p21(Cip1/WAF1) upregulates the Nrf2-mediated antioxidant response. Mol. Cell *34*, 663–673.

Dixon, S.J., Lemberg, K.M., Lamprecht, M.R., Skouta, R., Zaitsev, E.M., Gleason, C.E., Patel, D.N., Bauer, A.J., Cantley, A.M., Yang, W.S., et al. (2012). Ferroptosis: an iron-dependent form of nonapoptotic cell death. Cell *149*, 1060–1072.

Dixon, S.J., Patel, D.N., Welsch, M., Skouta, R., Lee, E.D., Hayano, M., Thomas, A.G., Gleason, C.E., Tatonetti, N.P., Slusher, B.S., and Stockwell, B.R. (2014). Pharmacological inhibition of cystine-glutamate exchange induces endoplasmic reticulum stress and ferroptosis. eLife *3*, e02523.

Ewald, J.C., Kuehne, A., Zamboni, N., and Skotheim, J.M. (2016). The yeast cyclin-dependent kinase routes carbon fluxes to fuel cell cycle progression. Mol. Cell *62*, 532–545.

Forcina, G.C., Conlon, M., Wells, A., Cao, J.Y., and Dixon, S.J. (2017). Systematic quantification of population cell death kinetics in mammalian cells. Cell Syst. *4*, 600–610.e6.

Jennis, M., Kung, C.-P., Basu, S., Budina-Kolomets, A., Leu, J.I.-J., Khaku, S., Scott, J.P., Cai, K.Q., Campbell, M.R., Porter, D.K., et al. (2016). An African-specific polymorphism in the TP53 gene impairs p53 tumor suppressor function in a mouse model. Genes Dev. *30*, 918–930.

Jiang, L., Kon, N., Li, T., Wang, S.-J., Su, T., Hibshoosh, H., Baer, R., and Gu, W. (2015). Ferroptosis as a p53-mediated activity during tumour suppression. Nature *520*, 57–62.

Johnson, L., Mercer, K., Greenbaum, D., Bronson, R.T., Crowley, D., Tuveson, D.A., and Jacks, T. (2001). Somatic activation of the K-ras oncogene causes early onset lung cancer in mice. Nature *410*, 1111–1116.

Johnson, T.M., Hammond, E.M., Giaccia, A., and Attardi, L.D. (2005). The p53QS transactivation-deficient mutant shows stress-specific apoptotic activity and induces embryonic lethality. Nat. Genet. *37*, 145–152.

Kruiswijk, F., Labuschagne, C.F., and Vousden, K.H. (2015). p53 in survival, death and metabolic health: a lifeguard with a licence to kill. Nat. Rev. Mol. Cell Biol. *16*, 393–405.

Lewerenz, J., Sato, H., Albrecht, P., Henke, N., Noack, R., Methner, A., and Maher, P. (2012). Mutation of ATF4 mediates resistance of neuronal cell lines against oxidative stress by inducing xCT expression. Cell Death Differ. *19*, 847–858.

Li, T., Kon, N., Jiang, L., Tan, M., Ludwig, T., Zhao, Y., Baer, R., and Gu, W. (2012). Tumor suppression in the absence of p53-mediated cell-cycle arrest, apoptosis, and senescence. Cell *149*, 1269–1283.

Maddocks, O.D.K., Berkers, C.R., Mason, S.M., Zheng, L., Blyth, K., Gottlieb, E., and Vousden, K.H. (2013). Serine starvation induces stress and p53-dependent metabolic remodelling in cancer cells. Nature *493*, 542–546.

Paek, A.L., Liu, J.C., Loewer, A., Forrester, W.C., and Lahav, G. (2016). Cell-to-cell variation in p53 dynamics leads to fractional killing. Cell *165*, 631–642.

Pfister, N.T., and Prives, C. (2017). Transcriptional regulation by wild-type and cancer-related mutant forms of p53. Cold Spring Harb. Perspect. Med. *7*, a026054.

Piskounova, E., Agathocleous, M., Murphy, M.M., Hu, Z., Huddlestun, S.E., Zhao, Z., Leitch, A.M., Johnson, T.M., DeBerardinis, R.J., and Morrison, S.J. (2015). Oxidative stress inhibits distant metastasis by human melanoma cells. Nature *527*, 186–191.

Stockwell, B.R., Friedmann Angeli, J.P., Bayir, H., Bush, A.I., Conrad, M., Dixon, S.J., Fulda, S., Gascón, S., Hatzios, S.K., Kagan, V.E., et al. (2017). Ferroptosis: a regulated cell death nexus linking metabolism, redox biology, and disease. Cell *171*, 273–285.

Tarunina, M., and Jenkins, J.R. (1993). Human p53 binds DNA as a protein homodimer but monomeric variants retain full transcription transactivation activity. Oncogene *8*, 3165–3173.

Vassilev, L.T., Vu, B.T., Graves, B., Carvajal, D., Podlaski, F., Filipovic, Z., Kong, N., Kammlott, U., Lukacs, C., Klein, C., et al. (2004). In vivo activation of the p53 pathway by small-molecule antagonists of MDM2. Science *303*, 844–848.

Wang, S.-J., Li, D., Ou, Y., Jiang, L., Chen, Y., Zhao, Y., and Gu, W. (2016). Acetylation is crucial for p53-mediated ferroptosis and tumor suppression. Cell Rep. *17*, 366–373.

Xie, Y., Zhu, S., Song, X., Sun, X., Fan, Y., Liu, J., Zhong, M., Yuan, H., Zhang, L., Billiar, T.R., et al. (2017). The tumor suppressor p53 limits ferroptosis by blocking DPP4 activity. Cell Rep. *20*, 1692–1704.

Cell Reports, Volume *22*

Supplemental Information

p53 Suppresses Metabolic Stress-Induced Ferroptosis in Cancer Cells

Amy Tarangelo, Leslie Magtanong, Kathryn T. Bieging-Rolett, Yang Li, Jiangbin Ye, Laura D. Attardi, and Scott J. Dixon

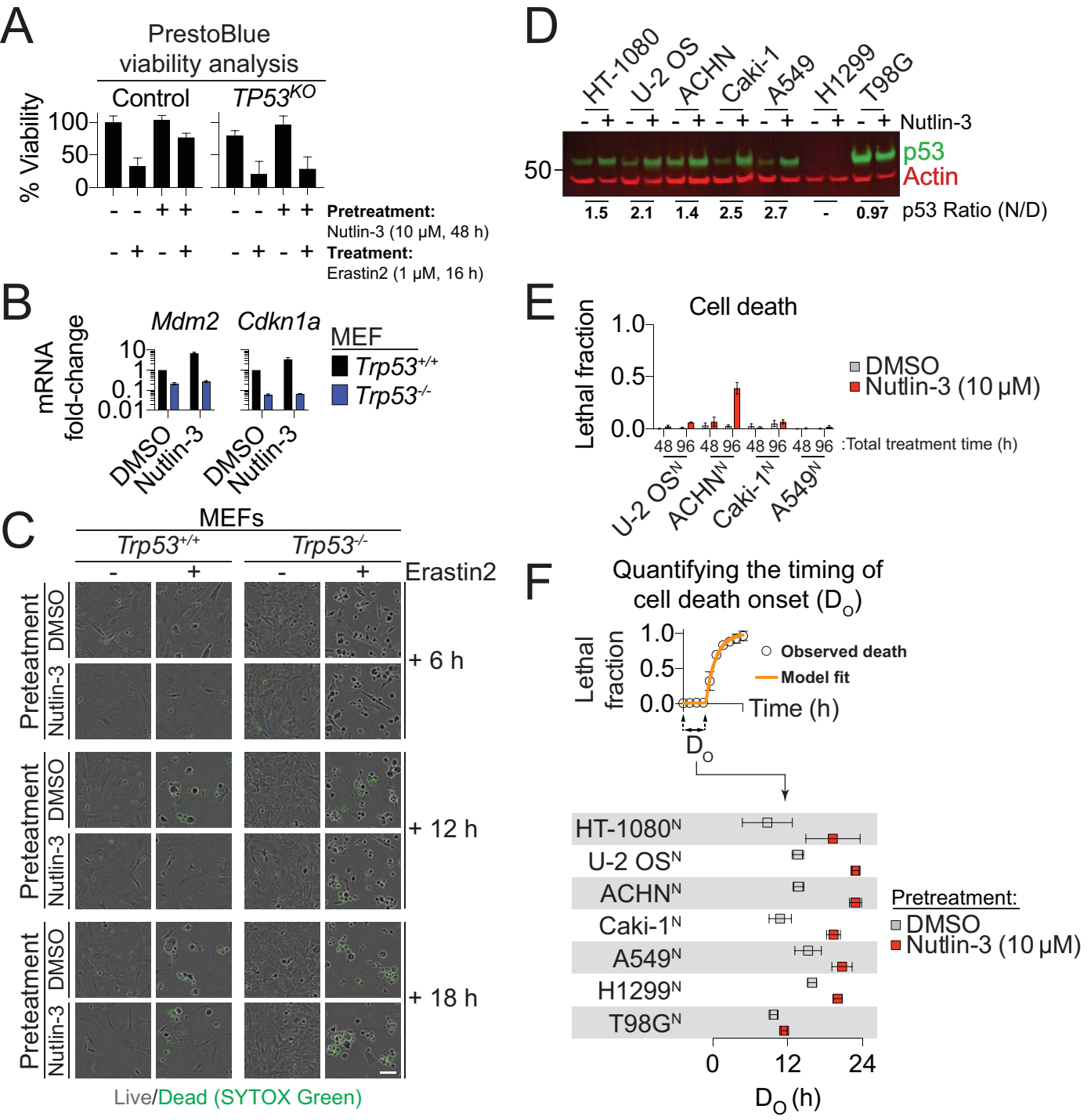

Supplemental Figure 1. p53 stabilization suppresses ferroptosis, Related to Figure 1. (A) Relative HT-1080 cell viability assessed using PrestoBlue at 16 h ± erastin2, following pretreatment ± nutlin-3. (B) Mdm2 and Cdkn1a levels in $p53^{+/+}$ and $p53^{-/-}$ MEFs. (C) Representative images of $Trp53^{+/+}$ and $Trp53^{-/-}$ MEFs pretreated ± nutlin-3 (10 μM, 48 h), then treated ± erastin2 (250 nM) and imaged at 6, 12 or 18 h in the presence of SYTOX Green. Images are representative of three independent experiments. The scale bar = 25 μm. (D) p53 levels ± nutlin-3 (10 μM, 48 h) in a panel of cancer cell lines. The actin-normalized ratio of p53 level in nutlin-3 versus DMSO treatment conditions is indicated. (E) Cell death following 48 h and 96 h ± nutlin-3 (10 μM) in four cell lines. (F) The timing of cell death onset (D_O) within the population can be quantified using STACK. D_O in a panel of cell lines in response to erastin2 (1 μM) ± nutlin-3 (10 μM, 48 h) pretreatment. Data represent mean ± SD from two (B) or three (A,E,F) biological replicates.

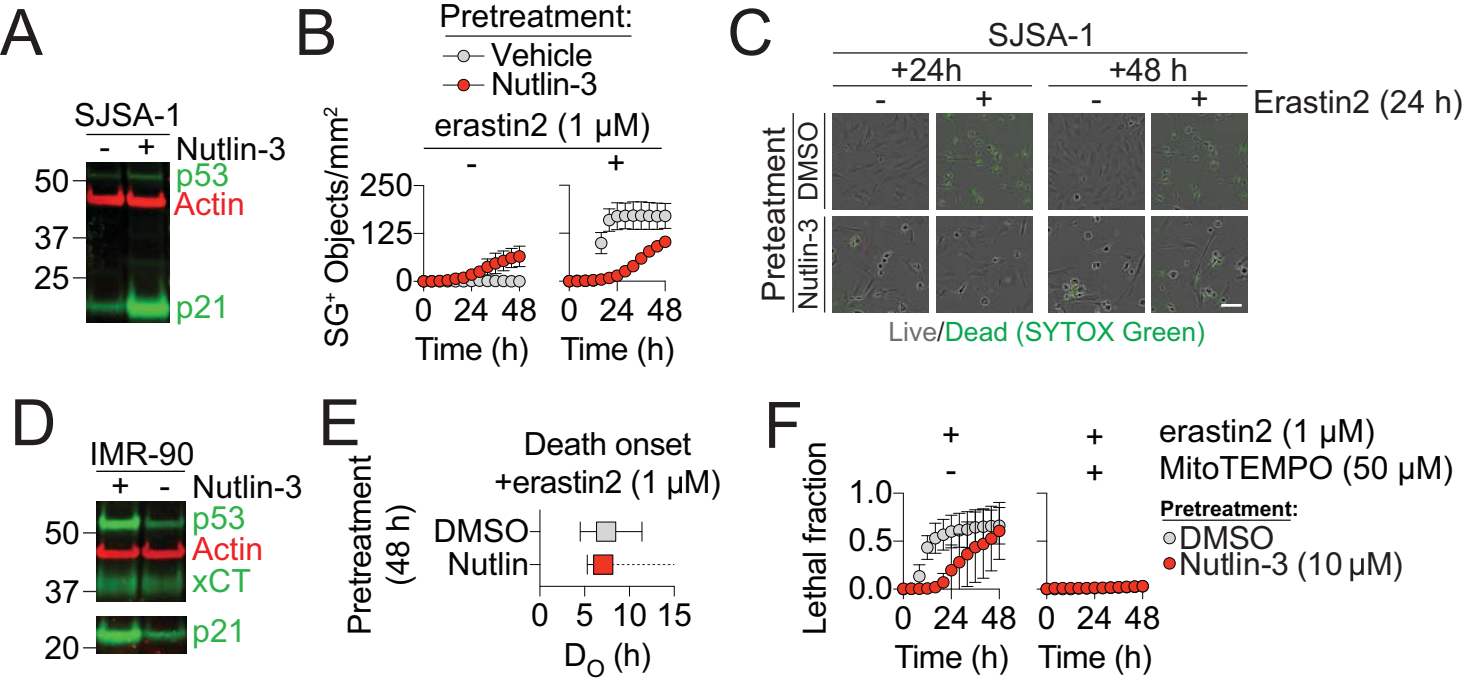

Supplemental Figure 2. Effect of p53 stabilization on ferroptosis, Related to Figure 1. (A) p53 and p21 levels in SJSA-1 cells ± nutlin-3 (10 μM, 24 h). (B) Dead cell (SYTOX Green, SG) counts over time in SJSA-1 cells ± erastin2 following pretreatment ± nutlin-3 (10 μM, 24 h). (C) Images from the experiments summarized in B, showing cell death at 24 and 48 h. The scale bar equals 25 μm. Note: the images for DMSO-pretreated, erastin2-treated cells at +24 h and +48 h appear highly similar as cell death is essentially complete by 24 h with little change thereafter. (D) p53, xCT and p21 levels in IMR-90 cells ± nutlin-3 (10 μM, 48 h). (E) Timing of cell death onset (D_O) ± 95% confidence interval in IMR-90 cells treated with erastin2 following pretreatment ± nutlin-3 (10 μM, 48 h). For nutlin-3-pretreated cells, the upper 95% confidence interval was not accurately resolved (indicated by the dotted line). (F) Cell death over time in HT-1080^N cells pretreated ± nutlin-3 (48 h) then treated with erastin2 ± mitoTEMPO. Unless otherwise indicated, data represent mean ± SD from three biological replicates. The brightness of the blots in A and D was increased uniformly to enable better

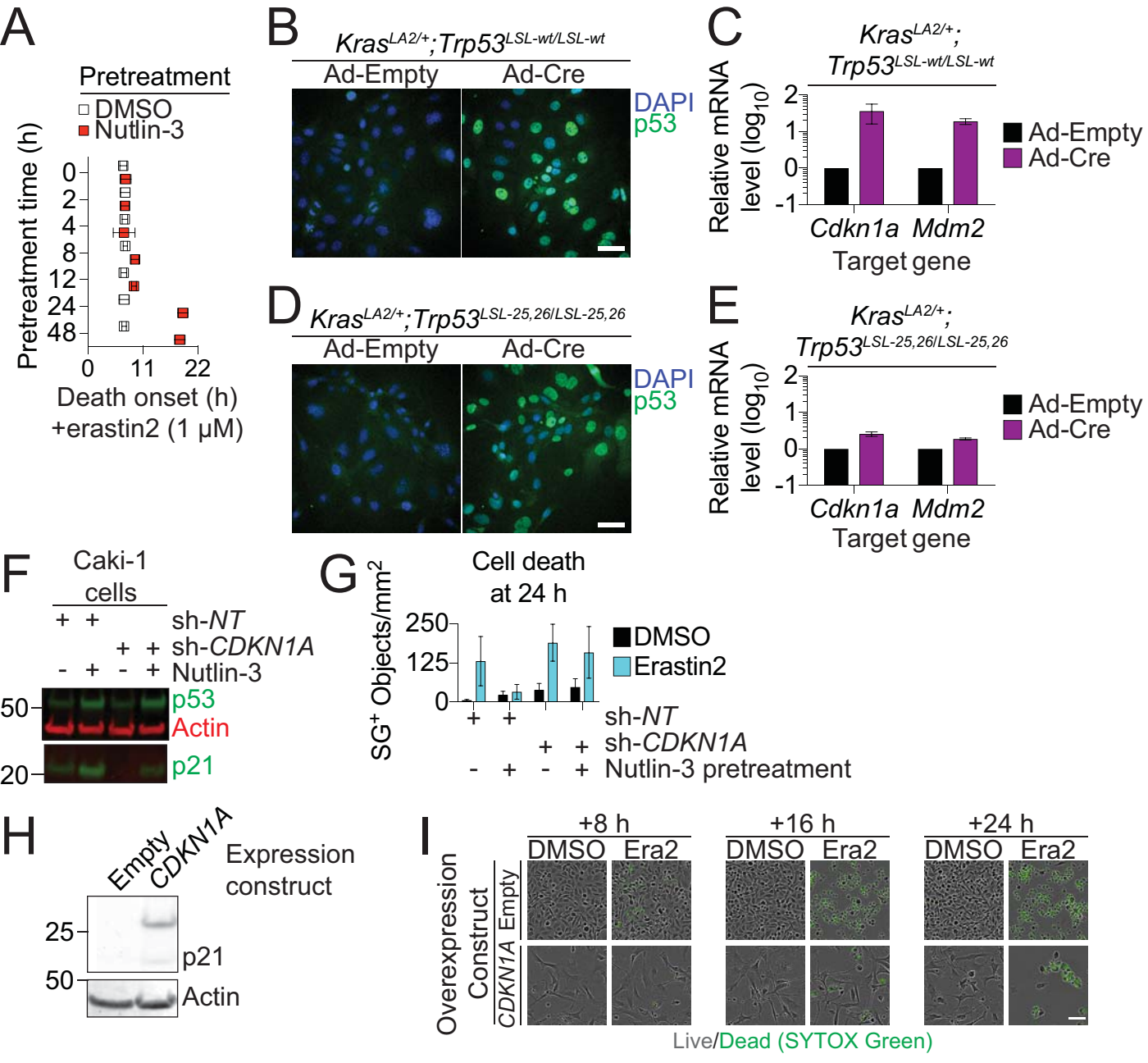

Supplemental Figure 3. p53-dependent transcription is necessary to suppress ferroptosis, Related to Figure 2. (A) Timing of cell death onset in HT-1080^{N} cells pretreated with nutlin-3 (10 μM) for various times. Data represent mean ± 95% confidence interval from two biological replicates. (B) p53 protein expression detected by immunohistochemistry following infection for 48 h with either an empty adenovirus (Ad-Empty) or an adenovirus directing the expression of Cre recombinase (Ad-Cre). Scale bar = 50 μm. (C) Relative gene expression following infection for 48 h with either Ad-Empty or Ad-Cre. (D) p53^{25,26} protein expression detected by immunohistochemistry following infection for 48 h with either Ad-Empty or Ad-Cre. Scale bar = 50 μm. (E) Relative gene expression following infection for 48 h with either Ad-Empty or Ad-Cre. (F) p53 and p21 levels in Caki-1 cells infected with a non-targeting shRNA (sh-NT) or shRNA targeting CDKN1A (sh-CDKN1A) ± nutlin-3 (10 μM). (G) SYTOX Green positive (SG^{+}) dead cell counts in Caki-1 cells infected and treated ± nutlin-3 for 48 h, as described in F, then treated ± erastin2 (1 μM) for 24 h. (H) p21 levels in HT-1080 cells infected with CMV-empty (Empty) or CMV-CDKN1A lentivirus for 48 h. (I) Representative images of HT-1080 cells infected as described in H and treated ± erastin2 (1 μM). Scale bar = 25 μm. Data in C, E and G represent mean ± SD from three biological replicates.

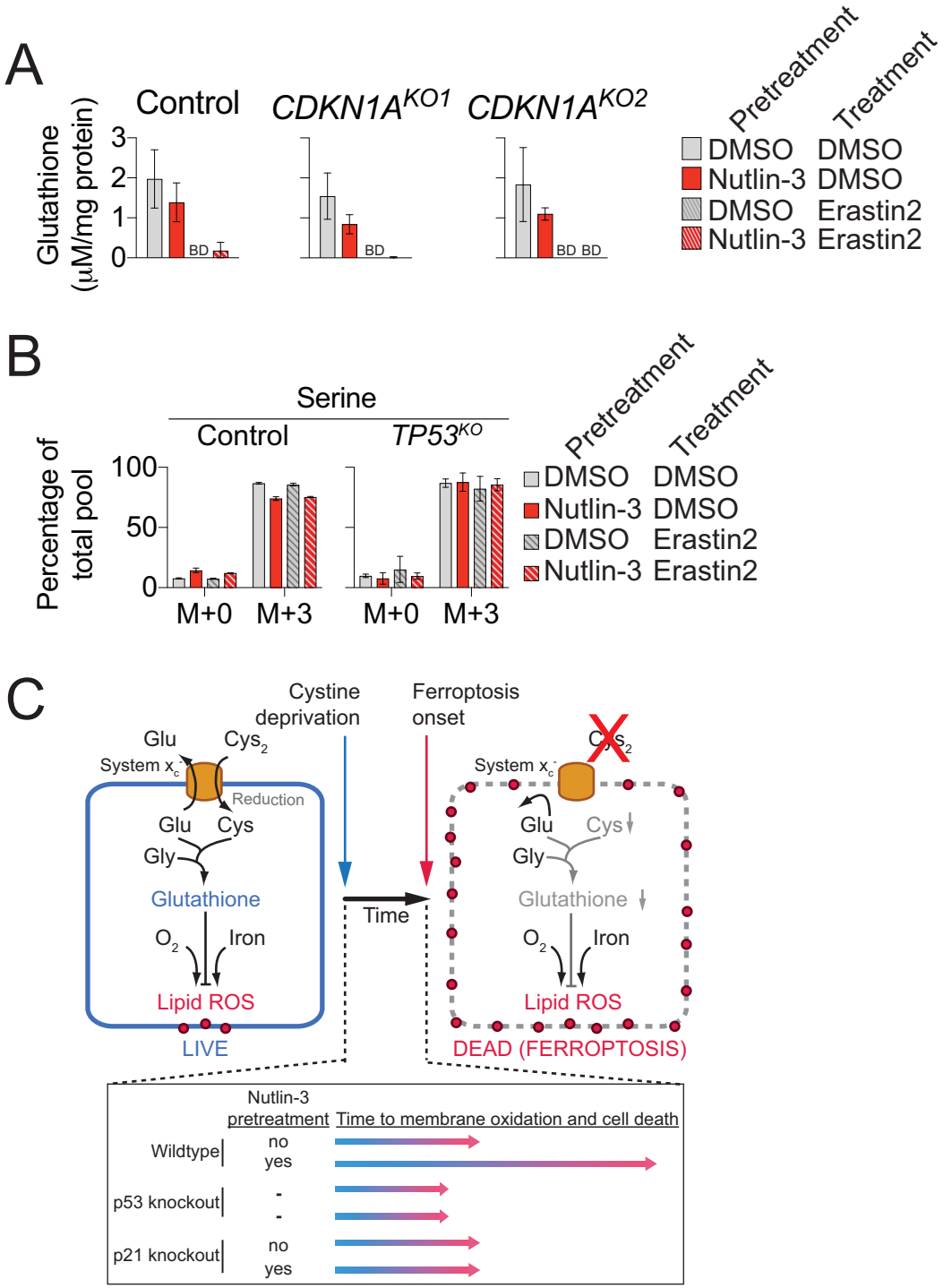

Supplemental Figure 4. p53 and GSH metabolism, Related to Figure 4. (A) Total glutathione levels in HT-1080 control and CDKN1A$^{KO1/2}$ cell lines measured using Ellman's reagent following pretreatment ± nutlin-3 (10 µM, 48 h) and treatment ± erastin2 (1 µM, 8 h). BD: below the limit of detection. (B) Unlabelled serine M+0 and labelled serine M+3 in HT-1080 control and TP53^{KO} cells pretreated ± nutlin-3 (10 µM, 48 h) then treatment ± erastin2 (1 µM, 8 h) in the presence of U-^{13}C-serine. Data in A and B represent mean ± SD from three independent biological replicates. (C) Model of p53 and p21 effects on the timing of lipid ROS accumulation and ferroptosis onset in response to system x_c^- inhibition and/or cystine deprivation.

Supplemental Experimental Procedures

Contact for Reagent and Resource Sharing

Further information and requests for resources and reagents should be directed to and will be fulfilled by the Lead Contact, Scott Dixon (sjdixon@stanford.edu).

Experimental Model and Subject Details

Cell Lines and Culture Conditions

HT-1080 (CCL-121), U-2 OS (HTB-96), A549 (CCL-185), CAKI-1 (HTB-46), ACHN (CRL-1611), T98G (CRL-1697), NCI-H1299 (CRL-5803), SJSA-1 (CRL-2098), IMR-90 (CCL-186) and 293T (CRL-3216) were obtained from ATCC (Manassas, VA, USA). HT-1080 cells were cultured in DMEM Hi-glucose medium (Cat# MT-10-013-CV, Corning Life Science) supplemented with 1% non-essential amino acids (NEAAs) (Cat# 11140-050, Life Technologies). U-2 OS, CAKI-1 and IMR-90 cells were cultured in McCoy's 5A media (Cat# MT-10-050-CV, Corning Life Science). A549, ACHN, T98G and 293T cells were cultured in DMEM Hi-glucose media. NCI-H1299 (referred to as H1299) and SJSA-1 cells were cultured in RPMI 1640 media with L-glutamine (Cat# SH30027FS, GE Healthcare). Polyclonal Nuc::mKate2-expressing HT-1080 cells (denoted HT-1080^{N}), as well as similar U-2 OS^{N}, A549^{N} and T98G^{N} cell lines were described previously (Forcina et al., 2017).

Method Details

Chemicals and Reagents:

Erastin2 (compound 35MEW28 reported in (Dixon et al., 2014)) was synthesized by Acme Bioscience (Palo Alto, CA, USA). Bortezomib (Cat# NC0587961), buthionine sulfoximine (Cat# AC23552-0010) and C11 BODIPY 581/591 (Cat# D3861) were from Thermo Fisher Scientific (hereafter Thermo Fisher). Nutlin-3 (Cat# S1061) was from Selleck Chemicals (Houston, TX, USA). Ferrostatin-1 (Cat# SML0583), mitoTEMPO (Cat# SML0737) and *tert*-butylhydroquinone (tBHQ, Cat# 112941) were from Sigma-Aldrich. Palbociclib was from SelleckChem (Cat# S1116, the kind gift of Dr. Julien Sage). Buthionine sulfoximine was dissolved directly into cell media. C11 BODIPY 581/591 was prepared as a stock solution in methanol and stored prior to use at -20˚C. All other compounds were prepared as stock solutions in DMSO and stored prior to use at -20˚C.

CRISPR/Cas9 gene editing

HT-1080 *TP53*^{KO} and *CDKN1A*^{KO} cell lines were generated as follows. A genomic region corresponding to exon 3 of human *TP53* and exon 2 of human *CDKN1A* was input into the CRISPR Design Tool (MIT, crispr.mit.edu). *TP53*: The following guides were selected based on a high quality score (97/100): Fwd- 5'-CCATTGTTCAATATCGTCCG, Rev- 3'-CGGACGATATTGAACAATGG. Overhangs (underlined) were added to each guide, yielding the following sequences: Fwd- 5'-CACCGCCATTGTTCAATATCGTCCG, Rev- 3'-AAACCGGACGATATTGAACAATGGC**.** *CDKN1A***:** The following guides were selected based on a high quality score (86/100): Fwd- 5'- TACCCTTGTGCCTCGCTCAG, Rev- 3'-CTGAGCGAGGCACAAGGGTA. Overhangs (underlined) were added to each guide, yielding the following sequences: Fwd- 5'- CACCGTACCCTTGTGCCTCGCTCAG, Rev- 3'- AAACCTGAGCGAGGCACAAGGGTAC**.** Guide RNAs were phosphorylated and annealed using T4 polynucleotide kinase (Cat# M0201S, New England Biolabs). The annealing reaction was incubated for 30 min at 37ºC, 95ºC for 5 min, then ramped down to 25ºC at a rate of 5ºC/min. Annealed primers were then diluted 1:200 in nuclease free water. Diluted annealed primers were then cloned into the pSpCas9(BB)-2A-GFP (PX458**,** Addgene, a kind gift from Dr. Jan Carette) plasmid using T4 DNA ligase (Cat# EL0014, Thermo Fisher). The ligation reaction was incubated for 6 cycles of 37ºC for 5 min followed by 21ºC for 5 min. To remove linearized DNA, the ligation product was treated with Plasmid-Safe DNase (Cat# E3101K, Epicenter) and incubated at 37ºC for 30 min, then 70ºC for 30 min. DH5α *E. coli* were transformed with the resulting ligation product and grown under ampicillin selection. Plasmid DNA was purified using the QIAprep Spin Miniprep Kit (Cat# 27106, Qiagen). Next, 1 µL of PolyJet (Cat# SL100688, SignaGen Laboratories) transfection reagent was used to transduce 50,000 HT-1080 cells seeded in 6-well format with 1 µg of pSpCas9(BB)-2A-GFP-sgRNA plasmids. Cells were incubated for 24 h, then GFP-expressing cells were sorted into single wells of a 96-well dish containing DMEM media with 30% fetal bovine serum on a BD InFlux cell sorter (Stanford Shared FACS Facility). Plates were monitored for three weeks for colony outgrowth. Colonies were dissociated using 0.25% trypsin-EDTA (Cat# 25200114, Thermo Fisher Scientific) and expanded up to 24-well plates, then to T-75 flasks. Genomic DNA (gDNA) was harvested from 0.5-2 x 10^6 cells using the QIAamp DNA Mini Kit (Cat# 51304, Qiagen). For validation of *TP53*^{KO} clones, a ~300 bp fragment from the *TP53* locus was amplified by PCR using the following primers: 5'-GCCAGGCATTGAAGTCTCAT-3' and 5'-GTCCCAAGCAATGGATGATT-3'. The PCR product was purified using the QIAquick PCR Purification Kit (Cat# 28106, Qiagen) and sequenced to screen for genetic disruption of the *TP53* locus with the following primer: 5'-TTCTGGGAAGGGACAGAAGATGACA-3'. A colony was identified in which a single base was

inserted at the expected cut site that resulted in a downstream premature stop codon. This clone was expanded and the absence of p53 protein was confirmed by Western blotting. For validation of *CDKN1A*^{KO} clones, cells growing in a T75 flask were dissociated using 0.25% trypsin-EDTA and approximately 1x10^6 cells were collected. Cells were pelleted and lysed in 9 M urea. Lysates were prepared and immunoblotted as described below (see *Immunoblotting)* to identify knockout cell lines.

Cell viability experimental design and set-up

Most experiments testing the effect of p53 stabilization on cell death used a pretreatment phase (24 or 48 h), with cells treated with either vehicle control (DMSO) or MDM2 inhibitor (e.g. nutlin-3). In all experiments a nutlin-3 concentration of 10 µM was used. Cell death was not assessed during this pretreatment phase. The unobserved pretreatment phase was followed by a treatment phase of 48 h where cell death observations were made, most often using scalable time-lapse analysis of cell death kinetics (STACK, (Forcina et al., 2017)) and cell lines expressing nuclear-localized mKate2 (e.g. control, *TP53*^{KO} and *CDKN1A*$^{KO1/2}$ HT-1080^N cells, Caki-1^N, H1299^N, etc). In some experiments, unmodified cells were employed and cell death was examined by SYTOX Green uptake alone (SJSA-1, IMR-90, mouse cancer cell lines). The detailed experimental set-up was as follows. On day 1, cells were seeded into clear bottom black 96-well plates (Cat# 07-200-588, Fisher Scientific). Cell seeding was optimized to ensure approximately equal cell numbers at the end the pretreatment phase (e.g. accounting for the fact that nutlin-3 treatment would arrest the proliferation of p53 wild-type cell lines but not p53 mutant cell lines). The following number of cells/well were used, for cells destined to be pretreated with either DMSO (D) or nutlin-3 (N): control HT-1080^N (D: 2000, N:4000), *TP53*^{KO} HT-1080^N (D: 1500, N:1500), *CDKN1A*$^{KO1/2}$ HT-1080^N (D: 2000, N:3000), U-2 OS^N (D: 2000, N: 4000), ACHN^N (D: 3000, N: 5000), Caki-1^N (D: 2000, N: 4000), H1299^N (D: 4000, N: 4000), T98G^N (D: 2500, N: 2500), A549^N (D: 5000, N: 5000), SJSA-1 (D:2000, N:4000), IMR-90 (D:5000, N:5000), *Trp53*$^{+/+}$ MEFs (D: 4000, N: 4000) and *trp53*$^{-/-}$ MEFs (D: 2000, N: 2000). On day 2, the start of the pretreatment phase, medium was exchanged and replaced with that containing either DMSO or MDM2 inhibitor (i.e. typically nutlin-3, 10 µM). On day 4 the medium was changed again and cells from both pretreatment conditions were then incubated in medium containing lethal compounds ± cell death inhibitors (e.g. ferrostatin-1) for an additional 48 h, until day 6. Note that either DMSO or nutlin-3 from the pretreatment phase was maintained in the medium during the treatment (observed) phase. Pretreatments were also performed using palbociclib (2 µM, 48 h). Cells for DMSO pretreatment were seeded at a density of 2000 cells/well, while those for palbociclib pretreatment were seeded at 3000 cells/well.

Cell death assessment using STACK

Cell death analysis was typically performed using STACK as follows. Following compound pretreatment or infection (e.g. adenovirus, shRNA), lethal compounds were added together with SYTOX Green viability dye (Cat# S7020, Life Technologies) at a final concentration of 22 nM. Cells were imaged at 2 or 4 h intervals for 48 h using the IncuCyte live cell analysis system (Essen BioScience). For cell lines stably expressing Nuc::mKate2 (e.g. HT-1080^N, ACHN^N), both mKate2 positive (mKate2$^+$) and SYTOX Green positive (SG$^+$) objects were counted using the IncuCyte ZOOM Live-Cell Analysis System software. Lethal fraction scores were computed for each time point, as described (Forcina et al., 2017). Lag exponential death (LED) curve fits to lethal fraction scores over time were obtained using Prism 6.0h (GraphPad, La Jolla, CA, USA), as described (Forcina et al., 2017). Time of cell death onset (a parameter value referred to as D_O) was obtained from LED curves fits, as described (Forcina et al., 2017). For experiments using cells not expressing Nuc::mKate2 cell death (SJSA-1, IMR-90, MEFs), cell death was measured by counting SG$^+$ objects over time. In some experiments, SG$^+$ counts were normalized between samples on a common scale using differences in starting cell confluence, inferred from phase-contrast images acquired in parallel, as a metric. Since long-dead cells can release SG (Forcina et al., 2017), the maximum SG$^+$ counts from the start of each time course were used in these calculations.

Transient cystine deprivation

The day before experiment, HT-1080^N control (60,000 cells/well for DMSO pretreatment and 120,000 cells/well for nutlin-3 pretreatment) and *TP53*^{KO} (40,000 cells/well for both pretreatments; we note that *TP53*^{KO} populations expand more quickly than control populations) cells were seeded in 6-well plates. The next day, cells were pretreated in cystine-replete medium with DMSO or nutlin-3 (10 µM). After two days, the cells were washed 3 times with HBSS, then treated with cystine-free medium + 20 nM SYTOX Green (except for the 0 h treatment, which was treated with cystine-replete medium + 20 nM SYTOX Green) + DMSO or nutlin-3 (10 µM). At a desired time point of cystine repletion, plates were imaged (IncuCyte Zoom) prior to replacing cystine-free medium + 20 nM SYTOX Green + DMSO or nutlin-3 (10 µM) with cystine-replete medium + 20 nM SYTOX Green. Note: population cell death was computed using the lethal fraction scoring approach which controls for the loss of SYTOX Green signal from long dead cells (Forcina et al., 2017). Thus, a decrease in the lethal fraction score over time from some maximum value can only be explained by an increase in the live cell numbers within the population (Forcina et al., 2017). Images were analyzed as described above.

PrestoBlue

In one experiment cell viability was assayed using PrestoBlue (Cat# A13262, Life Technologies). Cells were pre-treated with DMSO or nutlin-3 (10 μM) for 48 h as described above. Lethal compounds were then added and cells were incubated for a further 16 h. 10% final (v/v) PrestoBlue reagent was then added to existing media and mixed five times. Following 30 min incubation in a tissue culture incubator at 37°C, PrestoBlue signal was measured using a Synergy Neo2 reader (BioTek Instruments, Winooski, VT) at ex/em 530/590 nm. Background fluorescence from medium-only controls + 1x PrestoBlue was subtracted from all values and samples were normalized to an internal control treated with DMSO.

Adenovirus infection

For Western blot and RT-qPCR analysis, on day 1 murine $Kras^{LA2/+};Trp53^{LSL\text{-}wt/LSL\text{-}wt}$ and $Kras^{LA2/+};Trp53^{LSL\text{-}25,26/LSL\text{-}25,26}$ lung tumor cell lines cells were seeded into 6-well dishes. Given that we expected cells re-expressing p53 to stop proliferating, we initially seeded different numbers of cells such that by the end of 48 h we had roughly equivalent numbers for downstream assays. Thus, $Kras^{LA2/+};Trp53^{LSL\text{-}wt/LSL\text{-}wt}$ cells destined for infection with Ad-Empty were seeded at 1 x 10^5 cells/well, $Kras^{LA2/+};Trp53^{LSL\text{-}wt/LSL\text{-}wt}$ cells destined for infection with Ad-Cre were seeded at 2 x 10^5 cells/well, and $Kras^{LA2/+};Trp53^{LSL\text{-}25,26/LSL\text{-}25,26}$ cells destined for infection with either Ad-Empty or Ad-Cre were seeded at 1 x 10^5 cells/well. On day 2, cells were infected with either Ad5CMVempty (Ad-Empty, Cat# VVC-U of Iowa-272) or Ad5CMVCre (Ad-Cre, Cat# VVC-U of Iowa-5), obtained from the University of Iowa Viral Vector Core, at an M.O.I. of 100.

Cell death assays were conducted in 96-well plates. On day 1, cells were seeded at different numbers for reasons described above. Thus, $Kras^{LA2/+};Trp53^{LSL\text{-}wt/LSL\text{-}wt}$ cells destined for infection with Ad-Empty were seeded at 5000 cells/well, $Kras^{LA2/+};Trp53^{LSL\text{-}wt/LSL\text{-}wt}$ cells destined for infection with Ad-Cre were seeded at 7500 cells/well, and $Kras^{LA2/+};Trp53^{LSL\text{-}25,26/LSL\text{-}25,26}$ cells destined for infection with either Ad-Empty or Ad-Cre were seeded at 4000 cells/well. On day 2 cells were infected using virus at an M.O.I. of 100. On day 4, the medium was replaced with cell death assay medium containing SYTOX Green and test compounds as described above.

Immunofluorescence

On day 1, $Kras^{LA2/+};Trp53^{LSL\text{-}wt/LSL\text{-}wt}$ and $Kras^{LA2/+};Trp53^{LSL\text{-}25,26/LSL\text{-}25,26}$ cells were seeded on glass cover slips. $Kras^{LA2/+};Trp53^{LSL\text{-}wt/LSL\text{-}wt}$ cells destined for infection with Ad-Empty were seeded at 1 x 10^5 cells/well, $Kras^{LA2/+};Trp53^{LSL\text{-}wt/LSL\text{-}wt}$ cells destined for infection with Ad-Cre were seeded at 2 x 10^5 cells/well, and $Kras^{LA2/+};Trp53^{LSL\text{-}25,26/LSL\text{-}25,26}$ cells destined for infection with either Ad-Empty or Ad-Cre were seeded at 1 x 10^5 cells/well. On day 2, cells were infected as described above and incubated at 37°C for a further 48 h. On day 4, cells were washed with PBS and fixed in 4% paraformaldehyde for 15 min at room temperature. Cover slips were then washed three times with PBS and stored in PBS at 4°C. Cells were then permeabilized with 0.25% Triton-X in PBS for 10 min at room temperature and washed twice in PBS. CM5 anti-p53 antibody was diluted 1:200 in PBS with 1% BSA and added to cover slips for 30 min at 37˚C. Cells were then washed three times in PBS and a secondary antibody mix prepared by diluting donkey-anti-rabbit 488 antibody (1:2000) (Cat# A21206, Life Technologies) and DAPI (1:10,000) (Cat# D1306, Life Technologies) in PBS was added for 45 min. Slides were then washed three times with PBS and a drop of ProLong Gold antifade reagent (Cat# P36930, Thermo Fisher) was added and the coverslips were mounted on slides. Slides were allowed to dry overnight and sealed with nail polish. Images were acquired using a Zeiss Observer Z1 confocal microscope. Images were processed in ImageJ (National Institutes of Health, Bethesda, MA).

Image Analysis

Images were processed in Image J (version 1.50i) or Adobe Photoshop (Adobe Systems, San Jose, CA).

Immunoblotting

Cells were washed twice in HBSS (Cat# 14025-134, Life Technologies) and harvested using a cell scraper. Cell pellets were lysed in 9M urea and sonicated ten times using one-second pulses at maximum amplitude on a Fisher Scientific Model 120 Sonic Dismembrator (Thermo Fisher). Lysates were centrifuged at 15,000 rpm at room temperature for 15 min and supernatants were removed to exclude debris. Lysates were quantified by Bradford Assay using the Bio-Rad Protein Assay reagent (Cat# 5000002, Bio-Rad). Samples were prepared using NuPage Reducing Agent (Cat# NP0009, Thermo Fisher), NuPage LDS Sample Buffer (Cat# NP0007, Thermo Fisher) and dithiothreitol. Samples were incubated at 70˚C and run on pre-cast NuPage SDS 4-12% gradient gels in NuPage MES Running Buffer (Cat# NP0002, Thermo Fisher).

For xCT immunoblotting, cells were washed twice in HBSS (Cat# 14025-134, Life Technologies) and harvested with a cell scraper. Cell pellets were lysed in RIPA buffer containing 0.1% SDS (10mM Tris pH 7.5, 150mM NaCl, 1mM EDTA, 0.5% sodium deoxycholate, 0.1% SDS, 1% Triton X100) for 1 h on ice. Lysates were then sonicated as described above. Lysates were centrifuged for 20 min at 15,000 rpm at 4ºC. Supernatants were collected and quantified using a Pierce BCA Protein Assay kit (Cat# 23225, Thermo Fisher). Samples were prepared using 4x Laemmli buffer (Cat# 1610747, Bio-

Rad) and incubated 10 min at room temperature. Samples were then run on pre-cast 4-15% polyacrylamide gels (Cat# 4561084, Bio-Rad).

Gels were transferred using an iBlot Dry Blotting System (Cat# IB21001, Thermo Fisher). Membranes were blocked in Odyssey PBS Blocking Buffer (Cat# 927-40010, Li-Cor) for one hour and probed with primary antibodies. Primary antibodies used were against actin (Cat# SC-1616, I-19, Santa Cruz), human p53 (Cat #SC-126, DO-1, Santa Cruz), murine p53 (Cat# SC-6243, FL-393, Santa Cruz), murine p53 (Cat#NCL-L-p53-CM5p, CM5, Leica), xCT (Cat# 12691, D2M7A, Cell Signaling Technology), and p21 (Cat# 2947, 12D1, Cell Signaling Technology). Membranes were probed overnight at 4˚C or for 1 hour at room temperature with rocking. Membranes were washed three times for 5 min in Tris buffered saline (Cat# 0788, ISC BioExpress) with 0.1% Tween 20 (TBST) at room temperature with rocking. Samples were probed with secondary antibodies (Donkey anti-goat-680 Cat# 926-68024, Donkey anti-goat-800 Cat# 926-32214, Donkey anti-rabbit-680 Cat# 926-68023, Donkey anti-rabbit-800 Cat# 926-32213, Donkey anti-mouse-680 Cat# 926-68022, Donkey anti-mouse-800 Cat# 926-32212, Li-Cor) in Odyssey Buffer (Li-COR, Cat# 927-40100) with 0.1% SDS and 0.4% Tween 20 for 1 h at room temperature with rocking. Membranes were washed three times for 5 min in TBST Membranes were then imaged using a Li-COR Odyssey CLx imager.

Reverse transcription and quantitative polymerase chain reaction (RT-qPCR)

Following treatment, cells were washed twice in PBS, and scraped to harvest. Cell lysates were harvested and RNA extracted using a Qiashredder extraction column (Qiagen, Cat# 79654) and the RNeasy Plus RNA Extraction Kit (Cat# 74134, Qiagen). cDNA was generated using the TaqMan Reverse Transcriptase Kit according to the manufacturer's instructions (Cat# N8080234, TaqMan). Quantitative PCR reactions were prepared with SYBR Green Master Mix (Cat# 4367659, Life Technologies) and run on an Applied Biosystems QuantStudio 3 real-time PCR machine (Thermo Fisher). Relative transcript levels were calculated using the ΔΔCT method and normalized to the *ACTB* gene. qPCR primer sequences are provided in the Supplemental Materials.

siRNA Gene Knockdown

HT-1080 cells were reverse-transfected using an siRNA targeting human *SLC7A11* (Hs_SLC7A11_2 FlexiTube siRNA, Cat# SI00104902, Qiagen). AllStars Negative Control siRNA (Cat# 1027280, Qiagen) was used as a negative control. AllStars Hs Cell Death siRNA (Cat# 1027298, Qiagen) was used as a positive control for transfection efficiency. Transfection mixes were prepared using 5 nM siRNA and 2 µL Lipofectamine RNAiMAX Transfection Reagent (Cat# 13778075, Life Technologies) to total of 200 µL in Opti-MEM Reduced Serum Media (Cat# 31985-062, Life Technologies). Diluted siRNA was added to diluted lipofectamine. The combined mixture was added directly to empty 6 well dishes and incubated for 15 min at room temperature. 1 x 10^5 HT-1080 cells in suspension were then plated directly onto the transfection mixture and swirled to combine. Cells were incubated for 48 h prior to assays and plates were only used in assays if all cells in the Hs Cell Death siRNA positive control wells were dead.

shRNA and cDNA Overexpression Constructs

The PLKO.1 shRNA lentiviral plasmid targeting *CDKN1A* was from Sigma-Aldrich (Cat# TRCN0000287091). The PLKO.1 non-targeting shRNA control plasmid was from Addgene (Cat# 1864). cDNA from human *CDKN1A* (Genbank Accession # CV025498.1) in a pDONR223 vector was obtained from the human ORFeome V7.1 library (clone ID 2821049, a kind gift of Dr. Aaron Gitler). The cDNA was cloned into the pLenti-CMV-Puro DEST vector (Cat# w118-1, Addgene) using Gateway LR Clonase II Enzyme Mix (Cat# 11791-020 Thermo Fisher) and confirmed by sequencing. Plasmid DNA was isolated using the QIAprep Spin Miniprep Kit (Cat# 27106, Qiagen).

Lentiviral Production

Lentiviruses were generated in 293T cells as follows. 0.5 x 10^6 293T cells were seeded in a 6-well dish the day before the transfection. The following day, cells were transfected with 1000 ng of plasmid DNA, along with 250 ng pMD2.G (Cat# 12259, Addgene) and 750 ng psPax2 (Cat# 12260, Addgene) lentiviral packaging plasmids. 3 µL PolyJet (Cat# SL100688, SignaGen Laboratories) transfection reagent diluted in plain DMEM was added to diluted plasmid DNA to a final volume of 100 µL and incubated for 15 min at room temperature. The transfection mixture was then added dropwise to cells. After 24 h, lentivirus-containing media was harvested by collecting media from cells three times at > 8 h intervals. Viral media was then filtered through a 0.45 µM PVDF (Cat# SLHV033RS, Millex) syringe-driven filter unit and frozen at -80ºC until use.

CDKN1A shRNA silencing experiment

Caki-1 cells were seeded in a 96-well dish at 4000 (cells treated with control shRNA constructs and nutlin-3) or 2000 (all other treatments) cells/well and infected with lentiviruses carrying non-targeting shRNAs (sh-NT) or shRNAs targeting *CDKN1A* at an M.O.I. of ~1 in media containing 8 µg/mL Polybrene (source). Infected cells were then spun at 1000

rpm for 1 h at room temperature. The next day, virus-containing medium was removed and cells were incubated in medium containing puromycin (10 µg/mL) and DMSO or nutlin-3 (10 µM) for a further 24 h. Media was then removed and replaced with media containing SYTOX Green (0.022 µM), DMSO or nutlin-3 (10 µM), and DMSO or erastin2 (1 µM), and cell death was assayed for the subsequent 48 h using time-lapse imaging. Cell death was assessed by counting SYTOX Green positive cells over time.

CDKN1A overexpression experiment

HT-1080 cells were seeded in a 96 well dish at a density of 2000 cells/well. The following day, cells were infected with lentiviruses carrying an empty vector (pLenti-CMV-Puro-DEST) or a lentivirus directing expression of *CDKN1A* cDNA under a CMV promoter (pLenti-CMV-Puro-*CDKN1A*), generated as described above. Cells were infected at an M.O.I. of ~1 in media containing 8 µg/mL polybrene and spun at 1000 rpm for 1 h at room temperature. The next day, virus-containing medium was removed and replaced with medium containing 10 µg/mL puromycin. After 24 h, cells were treated with SYTOX Green (0.022 µM) and DMSO or erastin2 (1 µM) and cell death was assayed using time-lapse imaging of SYTOX Green positive cells.

To collect cell material for p21 immunoblotting, 1 x 10^5 HT-1080 cells/well were seeded in a 6 well dish. The following day, cells were infected with lentiviruses, as described above, in media containing 8 µg/mL polybrene. The following day, virus-containing medium was removed and replaced with medium containing 10 µg/mL puromycin. After 24 h, media was removed, cells were washed twice in PBS, and cells were scraped, spun at 1500 rpm for 2 min, and cell pellets harvested for Western blotting.

Cell Cycle Analysis

The day before the start of the experiment, 1 x 10^5 (DMSO) or 2 x 10^5 (nutlin-3, palbociclib) HT-1080 cells/well were seeded into 6-well plates. The next day, cells were treated with DMSO, nutlin-3 (10 µM, 48 h) or palbociblib (2 µM, 24 h). At the end of the treatment phase, cells were dissociated with 0.25% trypsin-EDTA (Cat# 25200114, Thermo Fisher), centrifuged at 1000 x g for 5 min, washed twice in HBSS (Cat# 14025-134, Life Technologies), and fixed in 70% ethanol. Cells were stored at 4ºC for up to three weeks. Cells were then pelleted, washed in DPBS lacking calcium or magnesium (Cat# CV-21-031, Corning), and treated with RNAse A (Cat# 19101, Qiagen) at 1:100 (v/v) and propidium iodide (Cat# P3566, Thermo Fisher) at 1:20 (v/v). Cells were then incubated 30 min at 37ºC, centrifuged, washed twice in DPBS, resuspended in DPBS, and strained through a filter-top tube (Cat# 352235, Corning). Cell cycle status was quantified using a BD FACSCalibur flow cytometer. Data were processed using FlowJo v10.1 (FlowJo, LLC).

Glutamate Release Assay

Glutamate release was assayed as described (Dixon et al., 2014). The day before the experiment, 1-2 x10^5 adherent cells were seeded in a 6-well dish. The next day, cells were washed twice in cystine uptake buffer (137 mM choline chloride, 3 mM KCl, 1 mM $CaCl_2$, 1 mM $MgCl_2$,5 mM D-glucose, 0.7 mM K_2HPO_4, 10 mM HEPES, 300 µM cystine, pH 7.4). Uptake buffer containing DMSO or nutlin-3 (10 µM) and DMSO or erastin2 (1 µM) was then added to cells and incubated for 60 min at 37ºC. Cell medium was then collected and added to a 96-well assay plate. For normalization purposes, cells were trypsinized in 0.25% trypsin-EDTA (Cat# 25200114, Thermo Fisher) and cell number was quantified using a Cellometer Auto T4 Bright Field Cell Counter (Nexcelcom, Lawrence, MA). Glutamate release was detected using the Amplex Red Glutamic Acid/Glutamate Oxidase Assay kit (Cat# A-12221, Thermo Fisher) as per the manufacturer's instructions. 10 µM H_2O_2 and 25 µM L-glutamate were included as positive controls. Fluorescence readings were recorded at ex/em 530/590 on a Synergy Neo2 reader (BioTek). Background fluorescence from blank uptake medium was subtracted and samples were normalized to cell number.

C11 BODIPY 581/591 Imaging

HT-1080 cells were seeded on glass coverslips placed in 6 well dishes at a density of 1x10^5 (DMSO treated) or 2x10^5 cells/well (nutlin-3 pretreated). Cells were pretreated with DMSO or nutlin-3 (10 µM) for 48 h. Media was then removed and replaced with media containing DMSO or nutlin-3 (10 µM), consistent with the respective pretreatment condition, and either DMSO or erastin2 (1 µM) for 10 h. At this point, cell media was aspirated and cells were washed with HBSS. A 5 µM working solution of C11-BODIPY was prepared in HBSS and added to cells for 10 min at 37ºC. The C11-BODIPY mixture was then aspirated and 1 mL of fresh HBSS was added to cells. To prepare cells for imaging, 25 µL of HBSS was pipetted onto a microscope slide lined with parafilm. Coverslips holding stained cells were then lifted out of plates using a needle tip and inverted onto prepared slides. Slides were then sealed with melted Vaseline. Slides were imaged on a Zeiss Observer Z1 confocal microscope and images were processed in ImageJ. Brightness for all images was auto-adjusted based on images with the brightest signal.

Biochemical Glutathione Detection Assay

Total glutathione was assayed as described (Dixon et al., 2014). Following treatment in 6-well dishes, cells were washed once with HBSS (Cat# 14025-134, Life Technologies) and collected into MES buffer with 1 mM EDTA using a cell scraper. Samples were sonicated ten times with one second pulses at maximum amplitude on a Fisher Scientific Model 120 Sonic Dismembrator (Thermo Fisher). Lysates were centrifuged at 14,000 rpm for 15 min at 4ºC. Supernatants were collected and protein was quantified by Bradford assay using the Bio-Rad Protein Assay reagent (Cat# 5000002, Bio-Rad). To deproteinate lysates, an equal volume of 12.5M metaphosphoric acid was added and incubated for 5 min at room temperature. Lysates were then centrifuged at 15,000 rpm for 3 min at room temperature and the resultant supernatants collected and stored at -20ºC. Total glutathione was measured using the Cayman Glutathione Assay kit (Cat# 703002, Cayman Chemical) per the manufacturer's instructions. Assay reading was performed on a Synergy Neo2 reader (BioTek). Results were normalized to total protein concentration for each sample.

Metabolic Flux Analysis

HT-1080 control (75,000 c/w for DMSO, 150,000 c/w for nutlin-3), *TP53*^{KO} (50,000 c/w for both DMSO and nutlin-3) and *CDKN1A*^{KO1} cells (75,000 c/w for DMSO, 100,000 c/w for nutlin-3) were seeded overnight in 6-well dishes in RPMI 1640 medium (Cat# SH30027FS, Fisher Scientific) containing 10% FBS and 1x Pen/Strep. The next day, pretreatment was initiated with DMSO or nutlin-3 (10 μM) for 48 h in RPMI 1640 medium. After 48 h, media was removed and cells were then incubated for 8 h in RPMI medium lacking glucose, serine, and glycine (Cat# R9660-02, TEKnova) supplemented with 30 mg/L L-Serine-^{13}C3 (Cat# 604887**,** Sigma-Aldrich) and 2000 mg/L D-glucose (Cat# G54000, Sigma-Aldrich) ± erastin2 (1 μM). DMSO or nutlin-3 (10 μM) conditions were maintained from the pretreatment phase. Unlabeled controls were incubated for 8 h in standard RPMI 1640 medium with DMSO or nutlin-3 (10 μM). Following the 8 h treatment phase, cells were washed twice in cold PBS and fixed in 80% cold LC/MS grade acetonitrile (Cat #A955-500, Fisher Scientific) for 5 min on ice. Cells were then scraped to collect, sonicated three times for 15 sec in a water bath, spun at 12,000 rpm for 10 min, and the resulting supernatants were stored at -80ºC. The resulting pellet was resuspended in 100 μl of 0.2 M NaOH and heated for 20 min at 95^{o}C with vortexing every 5 min. The dissolved proteinaceous solution was pelleted at maximum speed for 5 min and protein concentration in the supernatant was determined by BCA assay.

Quantitative LC-ESI-MS/MS analysis of cell extracts was performed using an Agilent 1290 UHPLC system equipped with an Agilent 6545 Q-TOF mass spectrometer (Santa Clara, CA, US). A hydrophilic interaction chromatography method (HILIC) with an BEH amide column (100 x 2.1 mm i.d., 1.7 μm; Waters) was used for compound separation at 35 °C with a flow rate of 0.3ml/min. The mobile phase A consisted of 25 mM ammonium acetate and 25mM ammonium hydroxide in water and mobile phase B was acetonitrile. The gradient elution was 0–1 min, 85 % B; 1–12 min, 85 % B → 65 % B; 12–12.2 min, 65 % B-40%B; 12.2-15 min, 40%B. After the gradient, the column was re-equilibrated at 85%B for 5min. The overall runtime was 20 min and the injection volume was 5 μL. Agilent Q-TOF was operated in negative mode and the relevant parameters were as listed: ion spray voltage, 3500 V; nozzle voltage, 1000 V; fragmentor voltage, 125 V; drying gas flow, 11 L/min; capillary temperature, 325 °C, drying gas temperature, 350 °C; and nebulizer pressure, 40 psi. A full scan range was set at 50 to 1600 (m/z). The reference mass were 119.0363 and 980.0164. The acquisition rate was 2 spectra/s. Isotopologues extraction was performed in Agilent Profinder B.08.00 (Agilent technologies). Retention time (RT) of each metabolite was determined by authentic standards (Table). The mass tolerance was set to +/-15 ppm and RT tolerance was +/-0.2 min.

Name	Formula	Mass(Da)	RT(Min)	METLIN	HMP	KEGG
Glycine	$C_2H_5NO_2$	75.032	6.96	20	HMDB00123	C00037
L-Serine	$C_3H_7NO_3$	105.043	7.56	30	HMDB00187	C00065
Glutathione	$C_{10}H_{17}N_3O_6S$	307.084	8.78	44	HMDB00125	C00051
Glutathione, oxidized	$C_{20}H_{32}N_6O_{12}S_2$	612.152	13.42	45	HMDB03337	C00127

Graphing and Figure Assembly

Graphing and all other statistical analyses were performed using GraphPad Prism 6.0h. The Results and individual Figure Legends contain additional statistical details. Figures were assembled using Adobe Illustrator.

Resource Table

REAGENT or RESOURCE	SOURCE	IDENTIFIER
Antibodies		
Anti-p53 (mouse) (CM5)	Leica	Cat# P53-CM5P-L

Donkey-anti-rabbit 488	Life Technologies	Cat# A21206
DAPI	Life Technologies	Cat# D1306
Anti-Actin (I-19)	Santa Cruz	Cat# SC-1616
Anti-p53 (human) (DO-1)	Santa Cruz	Cat# SC-126
Anti-p53 (mouse) (FL-393)	Santa Cruz	Cat# SC-6243
Anti-p53 (mouse) CM5	Leica	Cat# P53-CM5P-L
Anti-xCT (D2M7A)	Cell Signaling Technology	Cat# 12691
Anti-p21 (12D1)	Cell Signaling Technology	Cat# #2947
IRDye 680LT Donkey anti-Goat IgG	Licor	Cat# 926-68024
IRDye® 800CW Donkey anti-Rabbit IgG	Licor	Cat# 926-32213
IRDye® 800CW Donkey anti-Mouse IgG	Licor	Cat# 926-32212
IRDye® 680LT Donkey anti-Rabbit IgG	Licor	Cat# 926-68023
IRDye® 680LT Donkey anti-Mouse IgG	Licor	Cat# 926-68022
Bacterial and Virus Strains		
NucLight Red lentivirus reagent (EF1a, Puro) Nuclear-localized mKate2 (Nuc::mKate2)	Essen BioSciences	Cat# 4265
Ad5CMVempty	University of Iowa Viral Vector Core	Cat# VVC-U of Iowa-272
Ad5CMVCre	University of Iowa Viral Vector Core	Cat# VVC-U of Iowa-5
Biological Samples		
N/A		
Chemicals, Peptides, and Recombinant Proteins		
Sytox Green	Life Technologies	Cat# S7020
Erastin (Compound 13MEW76 in (Dixon et al., 2014))	(Dixon et al., 2014)	N/A
Erastin2 (Compound 35MEW28 in (Dixon et al., 2014))	(Dixon et al., 2014)	N/A
Buthionine sulfoximine	Fisher Scientific	Cat# AC23552-0010
Ferrostatin-1	Sigma-Aldrich	Cat# SML0583
mitoTEMPO	Sigma-Aldrich	Cat# SML0737
Nutlin-3	Selleck Chemicals	Cat# S8059
MI-773	Selleck Chemicals	Cat# S8059
Palbociclib	Selleck Chemicals	Cat# S1579
Etoposide	Thermo Fisher Scientific	Cat# 12-261-00
DAPI	Life Technologies	Cat# D1306
Polybrene	Sigma-Aldrich	Cat# H9268-5G
Puromycin	Life Technologies	Cat# A11138-03
PolyJet	SigmaGen Laboratories	Cat#SL100688
Propidium Iodide	Thermo Fisher	Cat# P3566
RNAse A	Qiagen	Cat#19101
Lipofectamine RNAiMAX Transfection Reagent	Life Technologies	Cat # 13778075
Critical Commercial Assays		
QIAshredder RNA Extraction Column Kit	Qiagen	Cat# 79654
RNeasy Plus RNA Extraction Kit	Qiagen	Cat# 74134
TaqMan Reverse Transcriptase Kit	TaqMan	Cat# N8080234
Cayman Glutathione Kit	Cayman Chemical	Cat # 703002
QIAprep Spin Miniprep Kit	Qiagen	Cat# 27106
QIAquick PCR Purification Kit	Qiagen	Cat# 28106

SYBR Green Master Mix	Life Technologies	Cat# 4367659
Gateway LR Clonase II Enzyme Mix	Thermo Fisher	Cat# 11791-020
Bradford Assay Kit	Bio-Rad	Cat# 5000002
BCA Protein Assay Kit	Thermo Fisher	Cat# 23225
Amplex Red Glutamic Acid/Glutamate Oxidase Assay Kit	Thermo Fisher	Cat# A-12221
PrestoBlue Cell Viability Reagent	Thermo Fisher	Cat# A13261
Deposited Data		
N/A		
Experimental Models: Cell Lines		
HT-1080	ATCC	CCL-121
HT-1080^{N}	(Forcina et al., 2017)	N/A
HT-1080 *Control*	This paper	N/A
HT-1080 *TP53*^{KO}	This paper	N/A
HT-1080 *CDKN1A*^{KO1}	This paper	N/A
HT-1080 *CDKN1A*^{KO2}	This paper	N/A
U-2 OS	ATCC	HTB-96
U-2 OS^{N}	(Forcina et al., 2017)	N/A
T98G^{N}	(Forcina et al., 2017)	N/A
A549^{N}	(Forcina et al., 2017)	N/A
Caki-1	ATCC	HTB-46
Caki-1^{N}	This paper	N/A
ACHN	ATCC	CRL-1611
ACHN^{N}	This paper	N/A
NCI-H1299 (referred to as H1299 in the manuscript)	ATCC	CRL-5803
NCI-H1299^{N}	This paper	N/A
Kras$^{LA2/+}$*; Trp53*$^{LSL\text{-}wt/LSL\text{-}wt}$	This paper	N/A
Kras$^{LA2/+}$*; Trp53*$^{LSL\text{-}25,26/LSL\text{-}25,26}$	This paper	N/A
293T	ATCC	CRL-3216
SJSA-1	ATCC	CRL-2098
IMR-90	ATCC	CRL-186
Trp53$^{+/+}$ primary MEFs	(Johnson et al., 2005)	N/A
Trp53$^{-/-}$ primary MEFs	(Johnson et al., 2005)	N/A
Experimental Models: Organisms/Strains		
N/A		
Oligonucleotides		
Human *ACTB* qPCR forward primer [ATCCGCCGCCCGTCCACA]	(Van Nostrand et al., 2014)	N/A
Human *ACTB* qPCR reverse primer [ACCATCACGCCCTGGTGCCT]	(Van Nostrand et al., 2014)	N/A
Human *CDKN1A* qPCR forward primer [CACCGAGACACCACTGGAGG]	(Huang et al., 2015)	N/A
Human *CDKN1A* qPCR forward primer [GAGAAGATCAGCCGGCGTTT]	(Huang et al., 2015)	N/A
Human *MDM2* qPCR forward primer [GAATCATCGGACTCAGGTACATC]	Primerbank	Accession NM_002392.5
Human *MDM2* qPCR reverse primer [TCTGTCTCACTAATTGCTCTCCT	Primerbank	Accession NM_002392.5
Human *SLC7A11* qPCR forward primer [GGGCATGTCTCTGACCATCT]	(Martin and Gardner, 2015)	N/A

Human *SLC7A11* qPCR reverse primer [TCCCAATTCAGCATAAGACAAA]	(Martin and Gardner, 2015)	N/A
Human *GCLM* qPCR forward primer [CATTTACAGCCTTACTGGGAGG]	Primerbank	Accession NM_002061.3
Human *GCLM* qPCR reverse primer [ATGCAGTCAAATCTGGTGGCA]	Primerbank	Accession NM_002061.3
Human *GCLC* qPCR forward primer [GGCGATGAGGTGGAATACAT]	(Rushworth et al., 2011)	N/A
Human *GCLC* qPCR reverse primer [GTCCTTTCCCCCTTCTCTTG]	(Rushworth et al., 2011)	N/A
Human *NQO1* qPCR Forward primer [GCCGCAGACCTTGTGATATT]	(Rushworth et al., 2011)	N/A
Human *NQO1* qPCR Reverse primer [TTTCAGAATGGCAGGGACTC]	(Rushworth et al., 2011)	N/A
Human *HMOX1* qPCR Forward primer [GGCCAGCAACAAAGTGCAAG]	Designed in PrimerBlast	N/A
Human *HMOX1* qPCR Reverse primer [TGGCATAAAGCCCTACAGCA]	Designed in PrimerBlast	N/A
Human *NRF2* qPCR Forward primer [GAGAGCCCAGTCTTCATTGC]	(Reichard et al., 2007)	N/A
Human *NRF2* qPCR Reverse primer [TGCTCAATGTCCTGTTGCAT]	(Reichard et al., 2007)	N/A
Murine *Actb* qPCR forward primer [TCCTAGCACCATGAAGATCAAGATC]	(Brady et al., 2011)	N/A
Murine *Actb* qPCR reverse primer [CTGCTTGCTGAT CCACATCTG]	(Brady et al., 2011)	N/A
Murine *Cdkn1a* qPCR forward primer [CACAGCTCAGTGGACTGGAA]	(Brady et al., 2011)	N/A
Murine *Cdkn1a* qPCR reverse primer [ACCCTAGACCCACAATGCAG]	(Brady et al., 2011)	N/A
Murine *Mdm2* qPCR forward primer [GGACTCGGAAGATTACAGCCTGA]	(Li et al., 2012)	N/A
Murine *Mdm2* qPCR reverse primer [TGTCTGATAGACTGTGACCCG]	(Li et al., 2012)	N/A
TP53 sgRNA #1 Forward Primer [CACCGCCATTGTTCAATATCGTCCG]	CRISPR Design Tool (http://crispr.mit.edu)	N/A
TP53 sgRNA #1 Reverse Primer [AAACCGGACGATATTGAACAATGGC]	CRISPR Design Tool (http://crispr.mit.edu)	N/A
CDKN1A sgRNA #1 Forward Primer [CACCGTACCCTTGTGCCTCGCTCAG]	CRISPR Design Tool (http://crispr.mit.edu)	N/A
CDKN1A sgRNA #1 Reverse Primer [AAACCTGAGCGAGGCACAAGGGTAC]	CRISPR Design Tool (http://crispr.mit.edu)	N/A
Hs_SLC7A11_2 FlexiTube siRNA	Qiagen	Cat# SI00104902
Allstars Negative Control SiRNA	Qiagen	Cat# 1027280
AllStars Hs Cell Death siRNA	Qiagen	Cat# 1027298
Recombinant DNA		
pSpCas9 (BB)-2A-GFP-sgRNA-p53	This paper	N/A
pLenti-CMV-Puro-*CDKN1A*	This paper	N/A
Other Plasmids		
pMD2.G	Addgene	Cat# 12259
psPax2	Addgene	Cat# 12260
pSpCas9 (BB)-2A-GFP	Addgene	Cat# PX458
pDONR223-*CDKN1A*	Human Orfeome V7.1	Clone ID 2821049

pLenti-CMV-Puro DEST	Addgene	Cat# w118-1
pLKO.1 sh*CDKN1A*	Sigma-Aldrich (Mission)	Cat# TRCN000287021
pLKO.1 shSCR	Addgene	Cat# 1864
Software and Algorithms		
Prism	GraphPad Software	N/A
Excel	Microsoft Corp.	N/A
FlowJo	FlowJo LLC.	N/A
Data availability		
N/A		

Supplemental References

Huang, X., Zhang, S., Qi, H., Wang, Z., Chen, H.-W., Shao, J., and Shen, J. (2015). JMJD5 interacts with p53 and negatively regulates p53 function in control of cell cycle and proliferation. Biochim. Biophys. Acta *1853*, 2286–2295.

Martin, L., and Gardner, L.B. (2015). Stress-induced inhibition of nonsense-mediated RNA decay regulates intracellular cystine transport and intracellular glutathione through regulation of the cystine/glutamate exchanger SLC7A11. Oncogene *34*, 4211–4218.

Reichard, J.F., Motz, G.T., and Puga, A. (2007). Heme oxygenase-1 induction by NRF2 requires inactivation of the transcriptional repressor BACH1. Nucleic Acids Res. *35*, 7074–7086.

Rushworth, S.A., Shah, S., and MacEwan, D.J. (2011). TNF mediates the sustained activation of Nrf2 in human monocytes. J. Immunol. *187*, 702–707.

Van Nostrand, J.L., Brady, C.A., Jung, H., Fuentes, D.R., Kozak, M.M., Johnson, T.M., Lin, C.-Y., Lin, C.-J., Swiderski, D.L., Vogel, H., et al. (2014). Inappropriate p53 activation during development induces features of CHARGE syndrome. Nature *514*, 228–232.